Vol. 21 • No. 15 • August 9 • 2011

www.afm-journal.de

ADVANCED FUNCTIONAL MATERIALS

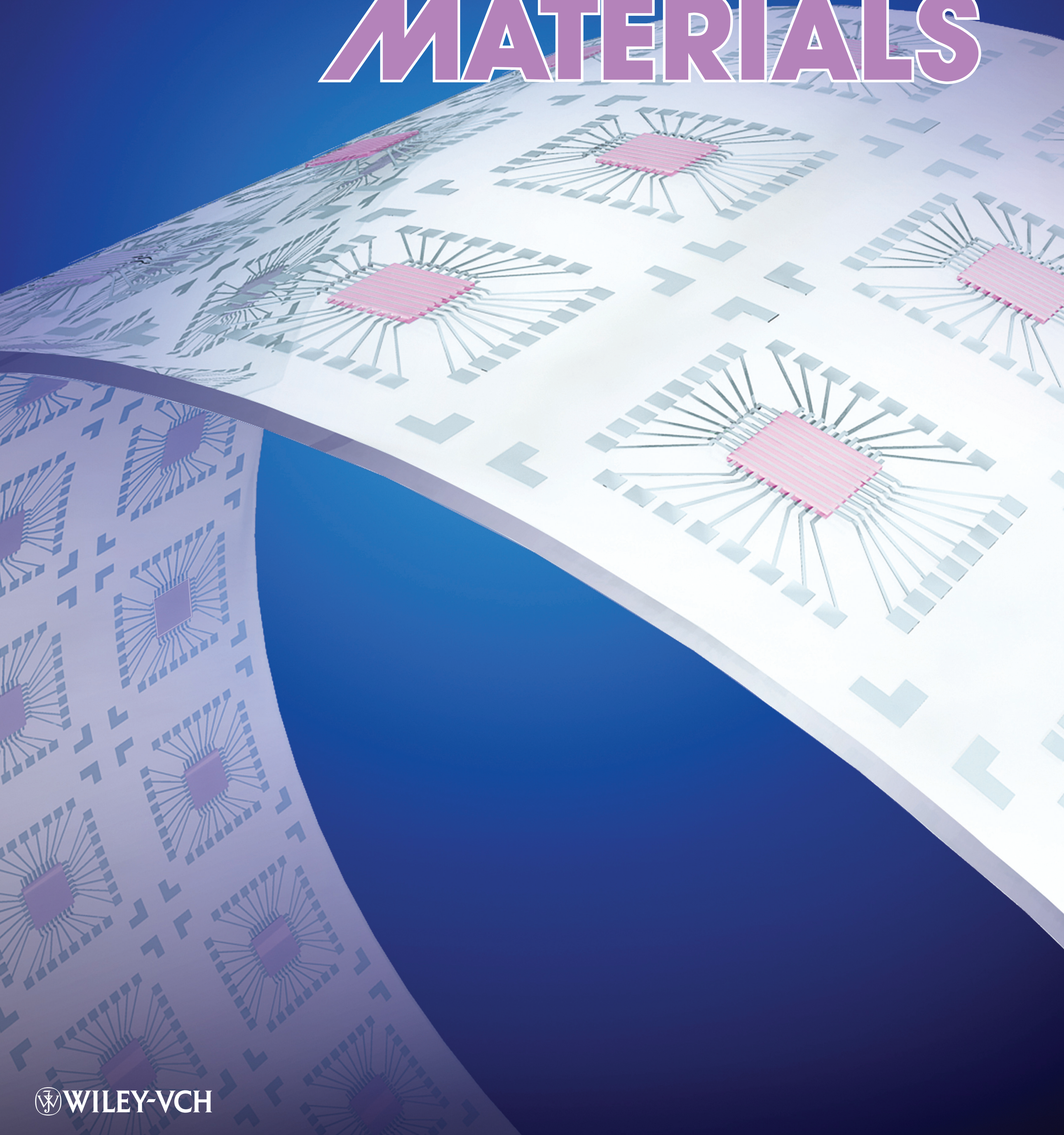

WILEY-VCH

Organic Resistive Memory Devices: Performance Enhancement, Integration, and Advanced Architectures

*Byungjin Cho, Sunghun Song, Yongsung Ji, Tae-Wook Kim, and Takhee Lee**

In recent years, organic resistive memory devices in which active organic materials possess at least two stable resistance states have been extensively investigated for their promising memory potential. From the perspective of device fabrication, their advantages include simple device structures, low fabrication costs, and printability. Furthermore, their exceptional electrical performances such as a nondestructive reading process, nonvolatility, a high ON/OFF ratio, and a fast switching speed meet the requirements for viable memory technologies. Full understanding of the underlying physics behind the interesting phenomena is still challenging. However, many studies have provided useful insights into scientific and technical issues surrounding organic resistive memory. This Feature Article begins with a summary on general characteristics of the materials, device structures, and switching mechanisms used in organic resistive devices. Strategies for performance enhancement, integration, and advanced architectures in these devices are also presented, which may open a way toward practically applicable organic memory devices.

1. Introduction

Because conventional Si-based technologies are common in the storage media market, the demands for higher integration densities and advanced device performance are continuously increasing. Si-based technologies are currently facing the theoretical and physical limits of downscaling. This hindrance to information storage has triggered the development of novel memory technologies that are principally based on the bistability of materials that arises from changes in intrinsic properties such as ferroelectricity, magnetism polarity, phase, conformation, and conductivity.[1–5] These emerging technologies include ferroelectric random access memory,[1] magnetoresistive random access memory,[2,5] phase-change random access memory,[3] and resistance random access memory (RRAM).[4,6] In particular, the organic-based RRAM developed by the Yang Yang group[7–12] is considered to be a promising candidate for next-generation nonvolatile memory devices.

Organic materials sandwiched between two vertically aligned electrodes constitute a memory device design in which the building blocks, referred to as bit cells, possess at least two stable resistance states that can be modulated by external electrical stimulation.[12–14] The use of organic materials provides many advantages including low fabrication costs, printability, and simple device structures. In organic resistive memory, resistance states can be read nondestructively, and no electrical power is required to maintain a given state of resistance, indicating a nonvolatile memory effect.[12–14] Furthermore, essential requirements for high performance memory, such as a fast switching speed and a high ON/OFF ratio, have been experimentally verified.[8,15] Although identifying the operating mechanisms is difficult, in-depth studies of charge conduction mechanisms, which have been facilitated by the development of advanced measurement techniques and analytical tools, have contributed to an understanding of the physics that underlie the switching phenomena. In addition to efforts undertaken to elucidate the origin of switching mechanisms, structural and electrical optimization concepts[15–28] have been used successfully to improve performance, further advancing the realization of more practical information storage devices. In Section 3 of this review, we highlight specialized technologies associated with memory performance enhancement, integration, and advanced device architectures. Because a variety of organic materials with bistability properties, switching behaviors, and operating mechanisms have already been described in recent literatures,[12–14] this review article focuses primarily on various strategies necessary for developing viable memory technologies.

This article includes four sections. Following the brief introduction to organic resistive memory devices in Section 1, Section 2 provides general background knowledge on the materials, device structures, switching characteristics, and switching mechanisms used in organic resistive switching. In Section 3, “Strategies for Memory Applications,” we propose several critical strategies for developing memory devices that have been electrically and structurally optimized. We suggest the following concrete strategies: memory performance enhancement

B. Cho, S. Song, Y. Ji, Prof. T. Lee
School of Materials Science and Engineering
Department of Nanobio Materials and Electronics
Gwangju Institute of Science and Technology
Gwangju 500–712, Korea
E-mail: tlee@gist.ac.kr
Dr. T.-W. Kim
Institute of Advanced Composite Materials
Korea Institute of Science and Technology
Jeollabuk-do 565–902, Korea

DOI: 10.1002/adfm.201100686

© 2011 WILEY-VCH Verlag GmbH & Co. KGaA, Weinheim

(interface tuning and active material tuning), high-density integration (downscaling and multi-bit), and advanced architectural concepts (active matrix systems, flexible memory application, and three-dimensional integration). Section 4 includes a summary and the current prospects for organic resistive memory devices.

2. Organic Resistive Switching

Various organic materials show bistable switching behaviors based on changes in resistance in two-terminal device structures.[9,12,19,21,24,29–54] Active organic materials such as small molecules, polymers, and composites, comprise the junction cells sandwiched between the bottom and top electrodes. A substantial amount of research has been dedicated to understanding the switching phenomena associated with these devices. Although the subject is still controversial, researchers have established several solid switching mechanisms based on theoretical simulations and experimental results. The reviews by Scott et al.[13] and Ling et al.[14] offer excellent discussions on various organic resistive memory devices. In this section, we provide a summary of the organic materials, common device structures, and switching characteristics of organic resistive memory devices. Mechanisms that have been proposed to describe the switching phenomena are also discussed.

2.1. Materials, Device Structures, and Switching Characteristics

Various organic materials show a change in resistance in response to an applied voltage.[9,12,19,21,24,29–54] Organic materials that exhibit conductance switching include small organic semiconducting molecules,[35–38,54] polymers,[12,39–45] and composites containing nanoparticles (NPs).[19,21,24,46–53] Thermal deposition and electrostatic self-assembly can be used to produce small molecular films.[35–38,54] Defective and poorly covered regions often appear in self-assembled monolayer (SAM) junction devices, preventing the establishment of reliable and reproducible electrical properties in molecular junctions sandwiched between electrodes. Although conductance-switching phenomena have been reported for several molecular devices,[35,55–58] the origin of the switching mechanisms is unclear, and research on these mechanisms is in its infancy. Thus, molecular-based memory is unlikely to become a viable technology in the near future. Compared to SAM molecules, many polymeric materials exhibit relatively uniform and robust film qualities and are more suitable for realistic memory applications. In addition, single-polymer-layer structures are more attractive due to the simplicity of device fabrication and the processability of solutions. Composite materials are commonly used to induce resistive switching.[19,21,24,46–53,59] Polymer-blending systems containing organic or inorganic NPs mainly constitute the active materials used in composite-based resistive memory devices. Conductance switching in organic memory devices including core-shell hybrid NPs has been also demonstrated.[48,53] Field-induced transfer of charge carriers was proposed to be responsible for the conductance switching.[48] In organic devices utilizing CdSe/ZnS NPs embedded in a conducting polymer, a bistable behavior was described on the basis of trapping, storing, and emission of charges in the electronic states of the CdSe NPs.[53] In these materials, resistance changes have been described to be caused by the introduction of NPs into the polymer matrix.[19,21,47–49,51,53,59] Thus, the concentration and agglomeration of NPs in a blending system are the most important fabrication parameters and must be carefully controlled during solution preparation.[19,29,46,59]

Byungjin Cho is a Ph.D. candidate in the School of Materials Science and Engineering, Gwangju Institute of Science and Technology (GIST), Korea. He graduated from Chungbuk National University, Korea, and received an M.S. degree in GIST in 2009. Since then, he has investigated two-terminal organic resistive memory devices. Currently, his research interests focus on resistive switching mechanisms and advanced architectures for practical memory applications.

Sunghoon Song received an M.S. degree in 2008 from the School of Materials Science and Engineering, Gwangju Institute of Science and Technology, Korea, where he is currently working toward his Ph.D. His current research interests are focused on the investigation of organic resistive memory switching mechanisms and the development of advanced architectures for practical organic memory integration.

Takhee Lee is a Professor in the School of Materials Science and Engineering, Gwangju Institute of Science and Technology, Korea. He graduated from Seoul National University, Korea, and received his Ph.D. from Purdue University, USA, in 2000. He was a postdoctoral researcher at Yale University, USA, until 2004. His current research interests are molecular electronics, polymer memory devices, nanowire electronics, and graphene-electrode optoelectronic devices.

© 2011 WILEY-VCH Verlag GmbH & Co. KGaA, Weinheim

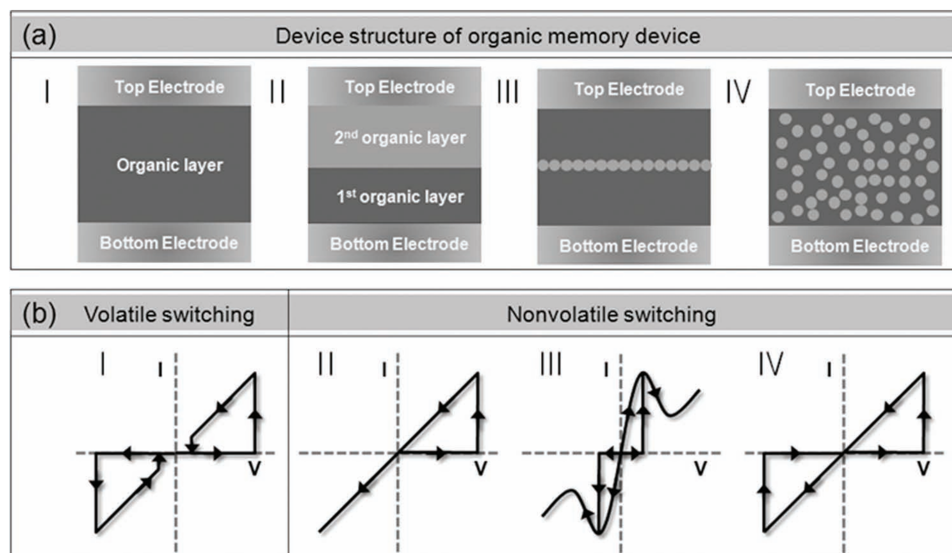

Figure 1. a) Typical structures of organic memory devices; I) a single-layer device without NPs, II) a bilayer structure containing two types of pure polymers, III) a structure in which the nano-traps are located in the middle of organic layer, and IV) spin-cast polymer-NP blends in which the nano-traps are randomly distributed throughout the entire thickness of the host matrix. b) Typical switching characteristics of organic resistive memory devices; I) *I–V* curve of DRAM-like volatile switching behavior, II) I–V curve of WORM switching behavior, III) I–*V* curve of unipolar switching, and IV) *I–V* curve of bipolar switching behavior.

In general, the following four device structures, which are classified by the configuration methods used to place active materials between electrodes, have been suggested for the fabrication of two-terminal organic resistive memory devices: I) a single-layer structure containing only one type of material and no NPs, II) a bilayer structure containing two types of polymers, III) a trilayer structure in which nano-traps are placed in the middle of the organic layer, and IV) spin-cast polymer-NP blends in which nano-traps are randomly distributed throughout the entire region of the host matrix (**Figure 1**a). The electrical switching characteristics of organic memory devices are categorized in two classes, volatile and nonvolatile switching, depending on the ability to retain information (Figure 1b). Similar to dynamic random access memory (DRAM), volatile switching requires periodic refreshing as a result of the loss of stored information.[60] Conversely, electrically programmed organic memory devices with nonvolatile switching characteristics can retain data for extended periods of time. This is similar to conventional flash memory. Nonvolatile switching is often classified into three types based on current-voltage (*I–V*) curves: write-once-read-many-times (WORM),[23,24,61,62] unipolar,[59,63] and bipolar switching memory[42,64] (II, III, and IV in Figure 1b). WORM-type memory devices[23,24,61,62] show electrically irreversible switching characteristics, and the original state is never recovered. These devices can be used as storage components for radio-frequency identification (RFID) tags. Both unipolar and bipolar memory systems exhibit electrically reversible switching. Unipolar memory devices use the same voltage polarity to write and erase,[59] while bipolar memory devices require different voltage polarities.[64] Unipolar memory devices have several technical advantages. For example, unipolar memory devices can be used to achieve electrically rewritable switching in architectures with one diode and one resistor (1D-1R) to prevent cross-talk interference.[65–68] Furthermore, the external circuits required in practical memory applications can also be simplified with the use of a single voltage polarity.

2.2. Mechanisms of Resistive Switching

Resistive memory devices are based on changes in the conductivity of a material that result when an electric field is applied. Conductivity is defined as the product of the carrier concentration and the charge mobility, and a change in the carrier concentration, charge mobility, or both, can lead to a change in conductivity. Although the origin of this change is unclear, each conductance state has been thoroughly described using the following well-established conduction mechanisms: ohmic conduction,[59] Schottky emission,[69] thermionic emission,[70–72] space-charge-limited current (SCLC),[36,70] tunneling current,[70,73] ionic conduction,[50,74] and hopping conduction.[71] In addition, the development of advanced analytical techniques has provided insight into switching phenomena.[31,36,37,49,61,75] Potential conductance and transition mechanisms have been proposed and partially established. In this section, we review the switching mechanisms of organic memory devices that have been reported and discussed previously. A recent review article contains a more extensive discussion of these mechanisms.[14]

2.2.1. Filamentary Conduction

Filamentary conduction occurs when the flow of current is limited to highly localized regions in a junction area.[76] Two types of filament paths have been suggested. One is associated with the carbon-rich filaments formed by the local degradation of organic films.[77,78] The other is related to the metallic

© 2011 WILEY-VCH Verlag GmbH & Co. KGaA, Weinheim

bridges that result from the migration of electrodes.[79,80] The filamentary switching mechanisms have been often suggested to explain resistive switching phenomena observed in a variety of organic memory devices. For example, Cu ions penetrated into organic layer under forward bias could result in filament formation in Cu/poly(3-hexylthiophene) (P3HT)/Al device, which was experimentally proved by secondary ion mass spectroscopy analysis.[75] Similar metallic filaments could also be formed in poly(ethylenedioxythiophene):poly(styrenesulfonate) (PEDOT:PSS) or poly(4-hydroxystyrene) composite materials that contain homogeneously dispersed Au clusters.[81] In the study, the stability and irreversibility of highly conductive percolation paths in a polymer resulted in WORM-type memory.[81] Meanwhile, electrical evidence of filamentary conduction has been reported in terms of metallic[82] and area-independent behaviors of high conductance state.[83] Indeed, nanoscale memory devices can be achieved in filamentary-based systems because switching occurs in highly localized regions, indicating the ease of downscaling.

2.2.2. Space Charge and Traps

If the contact between the electrodes and the organic material is ohmic and the insulator is trap-free, the accumulation of carriers near the electrode builds up a space charge. Mutual repulsion between individual charges restricts the total charge injected into a sample, and the resulting current is called SCLC.[84,85] Several factors contribute to this phenomenon: the injection of electrons or holes from the electrode, the presence of ionized dopants in interfacial depletion regions, and the accumulation of mobile ions at electrode interfaces. Traps present in the bulk of the material or at interfaces reduce carrier mobility. When the traps are located at interfaces, they can affect the injection of charges into a material. The electrical bistability of some organic materials has been reported to be associated with space charges.[43] For example, hysteresis in the *I–V* curves of an ITO/poly[3-(6-methoxyhexyl)thiophene]/Al structure was observed.[43] Bistable switching arises from the accumulation of space charges. The space charges accumulate at the metal–polymer interface and restrict the electrical field, which limits the injection of charges into the organic layer.[86] The stored charges control charge injection and lead to hysteresis in the *I–V* curve. Bozano et al.[87] discussed the switching phenomena of trilayer structures composed of granular metals sandwiched between two organic layers. They proposed that the switching phenomena are based on the charge storage mechanism described by Simmons and Verderber.[88] Specifically, bistable switching in the trilayer structures exhibits a negative differential region (NDR), causing bi- and multi-stability. At voltages in the NDR region, charges are tunneled into trapping sites, and a space-charge field builds up, inhibiting the field applied at the electrode and reducing current. Indeed, similar switching behaviors have been reported for many different materials in the same trilayer structure,[30,63,70] which provides the insight for the switching mechanisms.

2.2.3. Charge Transfer

Charge transfer occurs in electron donor–acceptor systems in which electrical charges are partially transferred from the donor to the acceptor moiety.[9,24,51,89] Field-induced transfers are expected to occur most frequently in the charge transfer complexes. Resistive switching of the complexes was observed in Cu-tetracyanoquinodimethane (TCNQ)[89]; Cu and TCNQ acted as the donor and acceptor, respectively. Raman spectroscopy measurements verified that pristine, high-resistance TCNQ anions were changed into neutral TCNQ molecules in a low-resistance state.[90] Chu et al.[9] also observed that the bistable resistance states of a [6,6]-phenyl-C61-butyric acid methyl ester (PCBM) and tetrathiofulvalene (TTF) dispersed in a polystyrene (PS) matrix were due to a charge transfer effect between the TTF and PCBM in the film. A strong electric field facilitated the transfer of electrons from the highest occupied molecular orbital of TTF to the lowest unoccupied molecular orbital of PCBM, producing a positive charge in TTF and a negative charge in PCBM. A sharp increase in conductivity occurred after the charge had been transferred.

2.2.4. Conformational Change

Resistive switching often arises from electrically induced conformational changes in molecules or molecular bundles.[35,41,54,61]For example, Rose Bengal (RB) molecules in supramolecular matrices of polyelectrolytes have shown conductance switching.[54] The conformational change effect responsible for this switching has been thoroughly described. In a low-voltage region, the reverse-bias-induced electro-reduction of RB molecules facilitates the restoration of conjugation in the backbone of the molecule, resulting in an ON state. With large biases, two perpendicular planes present in RB molecules induce a forward-bias-based conformational change and result in conductance switching. However, this switching phenomenon was not observed in devices made with RB spin-cast films.[91] This is because strong intermolecular interactions caused by the high packing density of the spin-coated film hindered conformational changes and rotations of molecular planes. A similar effect was also proposed for the resistive switching of poly(2-(9H-carbazol-9-yl)ethyl methacrylate) (PCz) and poly(9-(2-((4-vinylbenzyl)oxy)ethyl)-9*H*-carbazole) (PVBCz), which are non-conjugated polymers containing electron-donating carbazole pendant groups.[41,61] Upon application of an electric field, randomly oriented carbazole groups in the organic materials were rearranged into face-to-face conformations, thus facilitating carrier delocalization and transport and producing a high-conductance state. The difference in the memory behavior between PCz and PVBCz arose from inherent differences in the degree of regioregularity and the ease of conformational relaxation.

2.2.5. Ionic Conduction

Ionic conduction usually occurs in polymers containing ionic groups. Compared to the activation energy required for electronic conduction, the movement of ions requires a relatively high activation energy, and a long transit time of the ions is also expected. Electrically rewritable switching effects have been observed in P3HT[74] and a sexithiophene-poly(ethylene oxide) (6T-PEO) block copolymer.[50] Inorganic salts such as $LiCF_3SO_3$ and NaCl were used as dopants.[50,74] It has been

© 2011 WILEY-VCH Verlag GmbH & Co. KGaA, Weinheim

suggested that the migration of the dopant ions into and out of the P3HT or 6T-PEO depletion layer at the aluminum Schottky contact causes electrical bistability. In the case of 6T-PEO, the electrochemical doping of 6T occurs at both electrodes under a forward bias.[50,74] Near the Al electrode, 6T is reduced by the migration of sodium ions toward the metal electrode (n-type doping), while the oxidation of 6T occurs near the interface with the PEDOT:PSS electrode. This latter step is related to the migration of chloride ions in the vicinity of the interface (p-type doping).[50] These processes create a p-n junction and result in an asymmetrical I–V curve. Thus, rectifying bistable switching can be induced in organic systems using ionic conduction.

3. Strategies for Memory Applications

The viability of a memory technology is usually decided by the projected values of parameters such as the memory margin, switching speed, cycling endurance, retention time, and cell density. These parameters should enable organic memory devices to meet the minimum specifications necessary for next-generation memory applications. Uniform statistical data for these parameters, obtained from a large number of cells, are another essential requirement. This section, the core of this review article, presents essential strategies for practically implementing organic resistive memory devices. Three parts compose this section. In the first, we discuss various approaches to modulate switching characteristics and improve memory performance. In the second, we address the methods used to obtain high-density integration. Finally, advanced memory architectures, such as the active matrix system, flexible memory applications, and three-dimensional integration, are suggested.

3.1. Memory Performance Enhancement

3.1.1. Electrodes

The switching characteristics of organic resistive memory devices are strongly influenced by the properties of interfaces and active materials.[15–28] Accordingly, various approaches to control and optimize these switching properties have been applied.[15–28] In particular, the interface state between an electrode and an organic material influences the charge injection barrier, and new interfaces can be designed to adjust the electrical characteristics of organic devices.[92] The simplest method for modulating this interface is to change the type of electrodes used in organic resistive memory devices. The effects of different electrode combinations on conductance switching devices have been studied.[15] With a suitable electrode combination and as a result of a lowering of the injecting barrier height, a change in the conduction mechanism, and a decrease in the bulk resistance, improved conductance switching behavior (an ON/OFF ratio of approximately 10^7) was observed in an ITO/2,3-dichloro-5,6-dicyano-1,4-benzoquinone/Al device.[15] Additionally, the resistive switching voltage in polymer-metal nanoparticle films can be tuned by changing the work function of the electrode.[64] Specifically, the electrode sensitivity of the resistive switchings is due to the contact potential at the contact of gold nanoparticles and electrode arising from charge transfer between them.

The bistable switching effect can be altered depending on the metal deposition method.[45] Thermal deposition of Al has been reported to be more effective than electron-beam deposition in obtaining a high ON/OFF ratio and stable operation because of Al island growth, which is critical to memory performance and is dominant in thermally deposited Al films.[45] The flatness or geometrical shape of an electrode is also an important factor in terms of switching reproducibility.[27] For this reason, Lei et al.[27] statistically characterized polyfluorene-based memory cells and observed that switching probability was closely linked to the required switching voltage. Furthermore, they suggested that protrusions from the electrodes dominated the switching phenomena, and thus, their various geometries, led to errors in cycle testing. To reduce the probability of switching failure, a programming scheme that dynamically adjusts the switching voltages was designed. These researchers also stressed that a device structure with uniform bottom geometries should be devised to minimize changes in the switching sites, thus yielding a highly reliable and reproducible memory device.

3.1.2. Self-Assembled Monolayer and Nanodots

Introducing additional layers at the metal–polymer interfaces is an effective strategy for controlling the mobility or number of charge carriers that pass through organic devices. Among the types of layers that can be added, SAMs have attracted a substantial amount of attention due to simple and cost-efficient manner to change the interface property and then to modulate electrical property.[20,21,56,93] For instance, a hydroxyl-terminated Al electrode surface was treated with a 4-nitrophenyl dichloride phosphate SAMs. This treatment enhanced the switching reproducibility with a narrow distribution of the current level.[21] Similarly, Li et al.[20] investigated the influence of SAM molecules as an ultrathin potential barrier in an organic two-terminal structure. They characterized electrical switching behavior for the vertical charge transport through the organosilane of n-octyltrichlorosilane (OTS) embedded between two rubrene layers (**Figure 2**a,b). Although the OTS molecule, which consists of a saturated carbon backbone with a trichrolosilane end group, is dielectric in nature, high conductivity was observed in a sample that had been exposed for 6 h to OTS deposition and had no LiF layer (square line in Figure 2c). This result indicates the presence of defective regions with no or poor OTS coverage through which charges were actively transported. However, typical electrical switching behavior was observed in a sample that had been exposed for 6 h to OTS deposition and had a 15-nm LiF layer (curves 1–4 in Figure 2c). With a 450-fold increase in the current density, electrical switching suddenly occurred when the applied voltage was increased to 2.8 V. For an OTS deposition time of 15 or 30 min at the rubrene surface, negligible switching behavior was observed (Figure 2d). When the OTS deposition lasted for 2 and 6 h, 130- and 450-fold increases, respectively, were observed in the current densities at 1 V. The data for high- and low-conductivity states showed good fits to straight lines of the function $\ln J - V^{1/2}$ (inset in Figure 2d), indicating that conduction was mainly associated with the thermionic emission model.[72] This conductance transition was

© 2011 WILEY-VCH Verlag GmbH & Co. KGaA, Weinheim

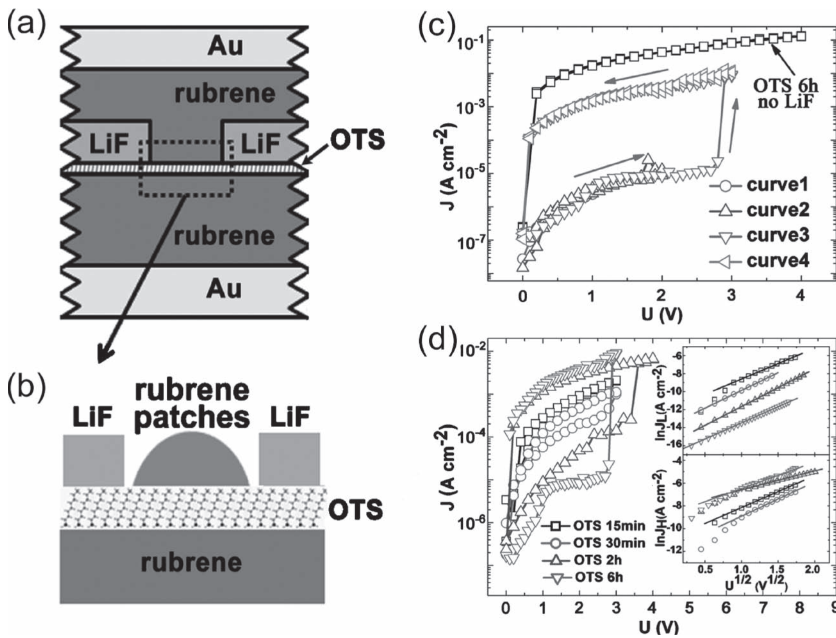

Figure 2. Schematic cross-section of a) the sample and b) the intergranular region between LiF grains, illustrating the formation of a discontinuous rubrene layer at the interface with the OTS layer during the early stages of deposition. c) Current density versus voltage (*J*–*V*) characteristics of the sample that was exposed for 6 h to OTS deposition and included a 15-nm LiF layer. The black square line represents the *J*–*V* characteristics of the sample that was exposed for 6 h to OTS deposition and had no LiF layer. d) J–V characteristics of samples with different OTS deposition times. The inset shows the *J*–*V* characteristics of the high-conductivity (top right) and low-conductivity states (bottom right). Reproduced with permission.[20] Copyright 2010, American Institute of Physics.

attributed to the potential OTS barrier, which can be tuned by changing the degree of OTS coverage on the rubrene layer. This result demonstrates the significance of self-assembly molecules in controlling vertical charge transport.

Kondo et al.[16] reported a method for improving memory performance by introducing charge-trapping layers. Three different types of devices were fabricated and compared. Device I consisted of a poly(N-vinylcarbazole) (PVK) layer embedded between two electrodes (ITO/PVK/Al) (**Figure 3**a). For device II, a similar structure was used, and Ag-nanodots (Ag-NDs) were added on the surface of the ITO substrate (ITO/Ag-NDs/PVK/Al) (Figure 3b). In device III, Ag-NPs (10 wt%) were dispersed in the PVK layer (ITO/PVK+Ag-NPs/Al) (Figure 3c). The ON/OFF ratios observed at a read voltage of 1 V were 20, 10^4, and 10^2 for devices I, II, and III, respectively (Figure 3d–f). Notably, the ON current values near the V_{max} region remained nearly constant regardless of the device type, while the OFF states were drastically affected by the presence of Ag-NDs or Ag-NPs. The nanomaterials added to device I played a critical role in enhancing the ON/OFF ratio, especially by reducing the current level in the OFF state. The authors explained that ON currents flowed through the low-resistance pathways of Al particles created in the PVK layer, while OFF currents were controlled by the charge-trapping layer of either Ag-NDs or Ag-NPs. Particularly, the Ag-NDs were much more efficient trapping sites than the homogenously dispersed Ag-NPs in the PVK layer.

3.1.3. Interfacial Oxide

A native oxide layer on an electrode surface sometimes seems to be necessary for resistive switching.[94,95] Furthermore, reproducible switching can be achieved by the introduction of an additional oxide film.[96] These observations validate the significance of the oxide layer in resistive switching memory. Similarly, we have investigated the effects of treating bottom Al electrodes with O_2 plasma on the switching characteristics of a polyimide (PI) composite material containing PCBM small molecules.[18] As shown in **Figure 4**a, the oxide thickness gradually increased as the treatment time increased. The increase in the oxide thickness was attributed to the time-induced enhancement of chemical reactions between Al atoms and oxygen molecules. X-ray photoelectron spectroscopy (XPS) depth profiles of the Al samples treated with O_2 plasma for different lengths of time (0, 5, 10, and 20 min) were compared (Figure 4b). In the graph, Al^m 2p and O 1s represent the metallic Al peak (Al–Al bonds) and the oxygen peak (Al–O bonds), respectively. As the plasma treatment time increased, the diffusion depth of oxygen gas into the Al layer gradually increased, indicating the formation of a thicker oxide layer. This is consistent with the transmission electron microscopy (TEM) data of Figure 4a. All of the devices tested showed typical unipolar switching behaviors, though their current levels differed depending on the plasma treatment time (Figure 4c). Both the ON and OFF resistance values gradually increased as the plasma treatment time increased (Figure 4d). Compared to the ON resistances, a relatively larger increase was observed in the OFF resistances, and this, in turn, produced a high ON/OFF ratio. This result indicates that the additional oxide served as a series resistor and considerably influenced the initial OFF resistance. The simple plasma treatment proposed in this study could be cost-effective because it does not require complex and expensive deposition equipment.

3.1.4. Organic Morphology

The importance of morphology in organic electronics has been emphasized because charge conduction through a device is often strongly governed by the surface morphology of an organic film.[92] For this reason, the morphology of the organic layer has been carefully controlled to produce excellent non-volatile memory effects.[17,23,28] For example, the deposition of a pentacene layer at a low deposition rate was found to play a definitive role in the occurrence of the resistive switching, while the deposition of a pentacene layer at a high deposition rate stabilized device performance.[23] Metal atoms can move inside an organic layer during the evaporation of the top electrode, and this inter-diffusion phenomenon strongly depends

© 2011 WILEY-VCH Verlag GmbH & Co. KGaA, Weinheim

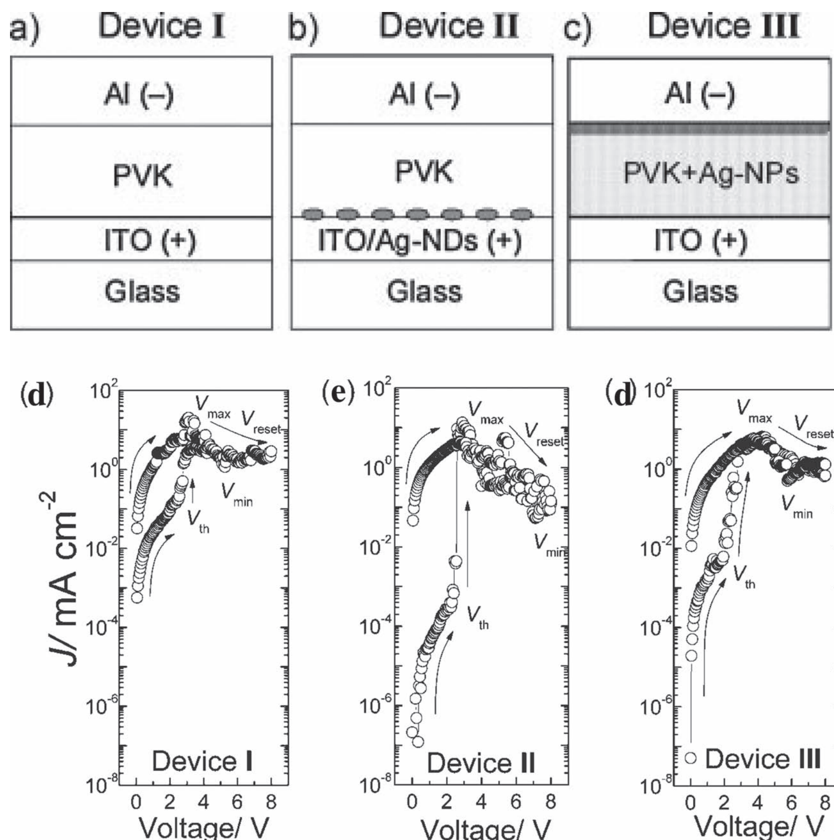

Figure 3. Schematics of three different device structures:[16] a) Device I includes a simple PVK layer embedded between two electrodes, with an ITO/PVK/Al structure; b) Device II consists of a similar structure but includes Ag-NDs on the surface of the ITO substrate and has an ITO/Ag-NDs/PVK/Al structure; c) Device III contains Ag-NPs (10 wt%) dispersed in the PVK composite and has an ITO/PVK+Ag-NPs/Al structure. Typical current density-voltage (*J–V*) characteristics for d) Device I with the ITO/PVK (150 nm)/Al structure, e) Device II with the ITO/Ag-NDs/PVK (150 nm)/Al structure, and f) Device III with the ITO/PVK+Ag-NPs (150 nm)/Al structure. In these figures, ITO and Al electrodes were used as the anode and cathode, respectively. Reproduced with permission.[16]

on the grain size of an organic film.[97] The deposition rate is one of the growth parameters that can be adjusted to change the grain size of pentacene films.[98] Thus, electrical characteristics in the organic memory were governed by the deposition rate of organic pentacene films.

Memory performance can be further improved with the use of new functional materials designed for nanomorphological control.[17] For instance, the material structures and electrical properties of devices fabricated with a nanoaggregated dispersed red 1-grafted poly(N-vinylcarbazole) (PVDR) and a non-nanoaggregated PVDR were characterized and compared.[17] Both devices exhibited a typical WORM memory effect, with a high ON/OFF ratio of more than 10^5 and a long retention time. However, the nanoaggregated PVDR device was much more stable than the non-nanoaggregated PVDR device. The surface defects and the large number of grain boundaries in the amorphous PVDR sample acted as charge-trapping centers, limiting mobility and degrading current in the ON state. Conversely, the helical columnar stacks that formed perpendicularly to the device electrodes in the self-assembled PVDR sample greatly enhanced electron delocalization via extended π–π interactions between the carbazole moieties in the polymer system. These π–π interactions provided an effective charge transport channel throughout the film. Moreover, the smoother surface of the nano-aggregated PVDR sample promoted better contact between the polymer and metal. These effects contributed to a much more stable ON current.

3.1.5. Composite Nanomaterials

Previous studies have shown that nanomaterials in various composite systems produce electrical bistability.[19,21,24,46–53] Generally, the electrical switching characteristics of memory devices fabricated with composite materials can be modulated by controlling the nanomaterial concentration. Laiho et al.[46] showed that a nanostructure of PCBM and PS enabled the facile tuning of switching behavior. With an increase in the PCBM concentration from 2 to 6 wt%, the switching voltage systematically decreased, while the unipolar switching curves including NDR region were observed across the entire concentration range. This was a result of the shorter average PCBM separation distance at higher concentrations. However, above 7 wt%, ohmic behavior was observed, but switching and NDR were not observed. The NDR region is an outcome of the tunneling process between PCBM clusters. Thus, cluster chains or single large clusters at high PCBM concentrations are believed to bridge two electrodes, resulting in a short-circuit current.

By controlling the carbon nanotube (CNT) content in PVK composite thin films, the electrical behavior of an ITO/PVK-CNT/Al structure can be tuned.[29] Distinctly different electrical conductance behaviors, such as insulator behavior, bistable conductance, and conductor behavior, were observed, depending on the CNT concentration in the PVK polymer. The controllable electrical properties and bistable switching effects in composite films have been attributed to electron trapping in the CNTs. Meanwhile, conjugated copolymers with doped CNTs have been shown to improve the performance of WORM memory behavior.[24] Doping the electroactive polymer layer with 1 wt% CNTs substantially enhanced device performance, e.g., a reduced turn-on voltage of –1.7 V and an enhanced ON/OFF ratio of 10^5. The lower energy barrier for charge transfer from the CNTs to the polymer contributed to the increase in the ON/OFF ratio, and the increased electron injection from the CNTs into the polymer lowered the turn-on voltage. Optimizing the ratio of Au-NPs in the PVK matrix was shown to improve current stability during constant stress tests.[19] Unwanted current fluctuations (e.g., sharp transitions from one state to another) during stress tests were observed for PVK-only devices and

© 2011 WILEY-VCH Verlag GmbH & Co. KGaA, Weinheim

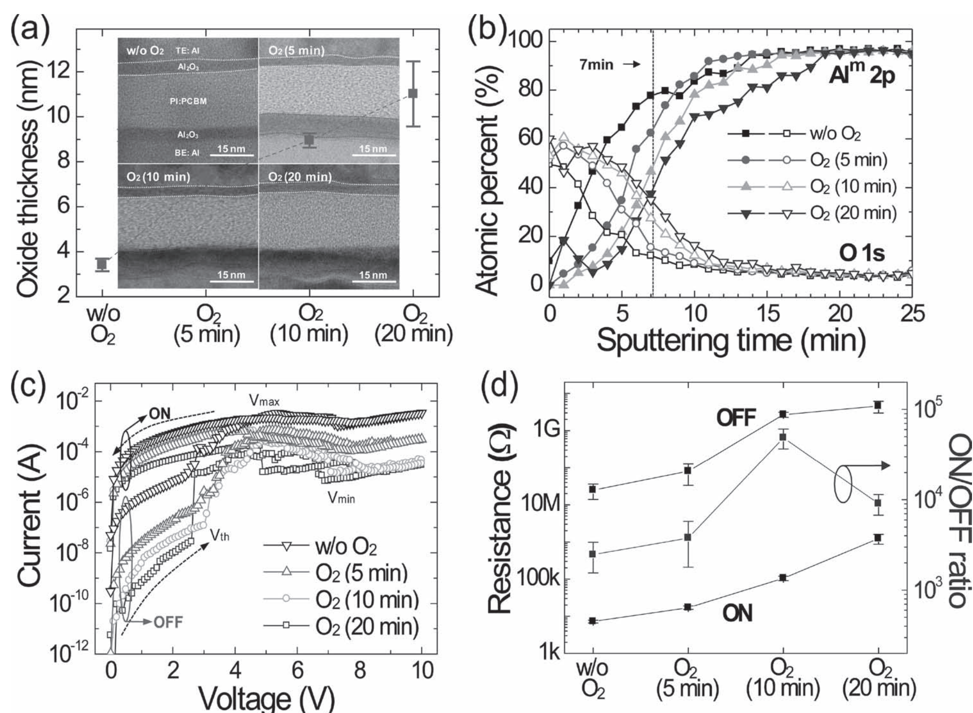

Figure 4. a) The thickness of Al oxide as a function of O_2 plasma treatment time: 0, 5, 10, and 20 min. The insets show TEM images of each memory device. The top and bottom pair of lines in each TEM image indicates the formation of the native Al oxide during deposition of the top electrodes and the interfacial Al oxide on the bottom electrodes created during plasma treatment, respectively. b) The XPS depth profiles of Al^m 2p and O 1s in the Al samples treated for varying times with O_2 plasma. c) *I–V* characteristics of organic memory devices treated with O_2 plasma for varying times. d) The ON and OFF resistances (left y-axis) and the ON/OFF ratios (right y-axis) as functions of the O_2 plasma treatment time. Reproduced with permission.[18] Copyright 2010, American Institute of Physics.

Au NPs:PVK = 0.2:1 devices, while good current stability was obtained for the Au NPs:PVK = 0.083:1 device. The role of Au NPs in this study was to store electrons donated from PVK. The proper amount of Au-NPs in the polymer-NP system stabilized the high-conductivity state.

3.1.6. Other Approaches

Other approaches for the modulation of active materials in organic resistive memory devices have been reported.[22,25,26,60,99,100] Chen and Ma[22,99] observed increases in the ON/OFF ratio after doping organic molecules with fluorescent dyes. To describe this effect, they proposed that doped fluorescent dyes in organic molecules act as trapping centers for charge carriers,[101] which improves the memory effect. A systematic study of organic bistable devices with the trilayer organic/metal-nanocluster/organic structure was performed by Pyo et al.[100] They observed an exponential decrease in the injection current of the ON state as the thickness of the organic layer increased, suggesting a decrease in the probability of electron transmission. Notably, the evolution from a current-step to bistability occurred above the critical thickness (10 nm) of an Al nanocluster. This phenomenon was described by a shift in the conduction mechanism from charge injection and trapping to resonant tunneling and charge storage. Meanwhile, the location of the middle metal layer in the trilayer structure, which consisted of 4,4′,4′′-tris[N-(3-methylphenyl)-N-phenylamino] triphenylamine (m-MTDATA) containing an ultra-thin Ag film, was also found to be an important processing parameter to determine memory performance.[25] Bottom and top electrode of the devices were ITO and Al, respectively. For devices in which the Ag film was located at the ITO/m-MTDATA interface, the largest ON/OFF ratio was observed, despite poor cycling endurance. However, for devices in which the Ag film was located in the middle region of the m-MTDATA layer, better endurance cycling was obtained, but the ON/OFF ratio was reduced. When the Ag film was near the Al electrode, the ON/OFF ratio and retention time of the devices decreased sharply. This result suggests that changing the location of the middle metal layer in the polymer can be used to modulate memory parameters (ON/OFF ratio, endurance, retention, and so on)

We recently found that the introduction of metal ions into the polymer can change the switching speed.[26] Poly[(9,9-bis((6′-(N,N,N-trimethylammonium)hexyl)-2,7-fluorene)-alt-(9,9-bis(2-(2-methoxyethoxy)ethyl)-fluorene)] dibromide (WPF-oxy-F) and its derivatives (Ca-WPF-oxy-F and Na-WPF-oxy-F) were synthesized[102] and used as active layers for our organic memory devices (**Figure 5**a–c). The device structure consisted of p^+ Si/polymers/Ag layers (Figure 5d). The cell size dependence of both the high-resistance state (HRS) and low-resistance state (LRS) was explored, as shown in Figure 5e. The resistance of the polyfluorene derivative with metal ions (Ca- and Na-WPF-oxy-F) clearly scaled with the cell size, indicating that the current flowed through the whole cell area in the HRS.[103]

© 2011 WILEY-VCH Verlag GmbH & Co. KGaA, Weinheim

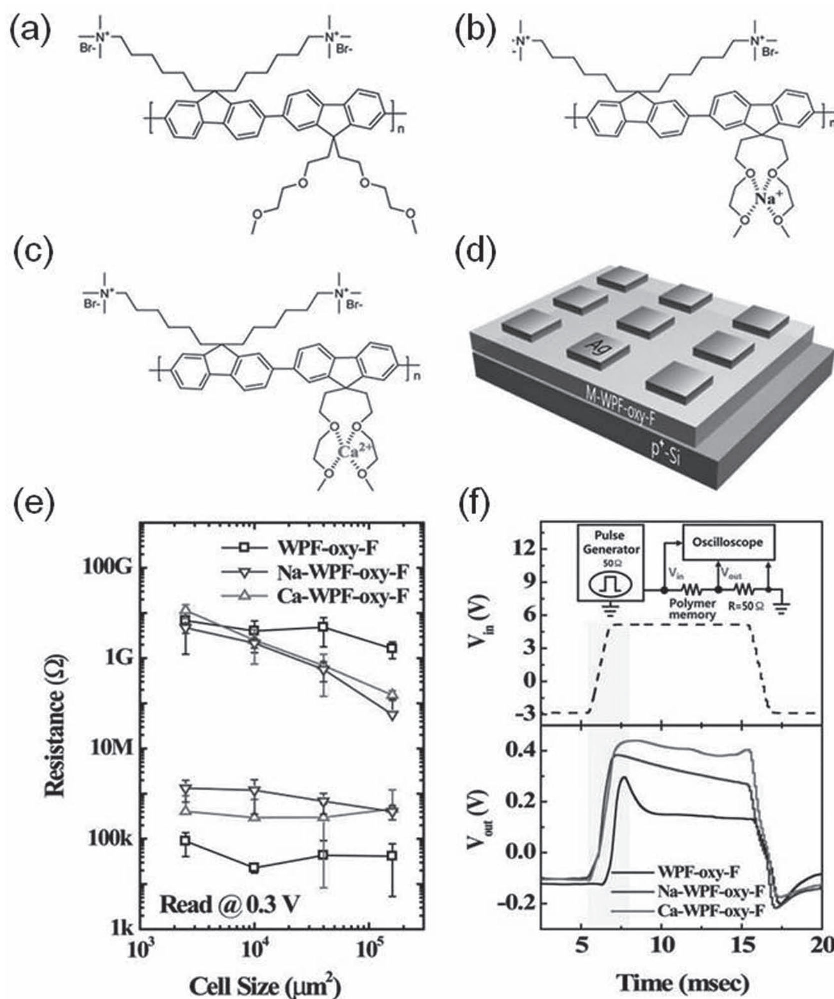

Figure 5. Chemical structures of polyfluorene-derivatives a) WPF-oxy-F, b) Na-WPF-oxy-F and c) Ca-WPF-oxy-F. d) Schematic of MIM-type organic nonvolatile memory device. e) Resistance values of the ON and OFF states of the three types of polyfluorene-derivative memory devices as a function of junction area. f) Transient response characteristics of the three types of devices. The inset shows the circuit of measurement method. Reproduced with permission.[26] Copyright 2010, Elsevier.

However, the resistance values of the three polymer materials in the LRS did not change significantly with cell size due to the formation of localized current paths.[104] However, unlike the results for Ca- and Na-WPF-oxy-F devices, HRS in WPF-oxy-F devices did not show any clear size dependence as a result of the SCLC and localized current flows.[31] To further study the effects of metal ions on memory performance, we measured the transient response times of the three types of polymer memory devices. The transient responses of Ca- and Na-WPF-oxy-F were fast (approximately 10 μs writing process), while WPF-oxy-F showed a much slower response time of approximately 2 ms (Figure 5f). The relatively fast switching time of WPF-oxy-F derivatives was due to the formation of conductive paths by metal ions within the polymers.

Lee et al.[60] found that the thickness of polymer films influenced the switching type. A fully π-conjugated polymer, poly(diethyl dipropargylmalonate), showed different electrical *I–V* curves, depending on the film thickness. Specifically, a polymer film with a thickness of 32 nm exhibited reliable WORM memory characteristics because localized filaments were stable at this thickness. However, the filaments in relatively thicker films (62 and 100 nm) were less stable, and DRAM characteristics were observed.

3.2. High-Density Integration

3.2.1. Downscaling Techniques

Organic-memory research has focused primarily on demonstrating bistable switching in existing or synthesized organic materials. However, the essential step for practical memory applications is to integrate the maximum number of memory cells into a single chip. To achieve this purpose, a considerable amount of effort has been devoted to the development of lithographic tools.[105,106] Generally, conventional lithography techniques require a solution process to develop or remove the photoresist. Because inorganic materials are robust against organic solvents, the well-established lithographic processes are suitable for the fabrication of inorganic-based memory devices. However, the use of the solution process dissolves the organic active layer on the substrate, thus rendering this process unsuitable for the downscaling of cell size in organic memory devices.

As an alternative method, we recently devised a via-hole structure that can be used as a scalable test bed to characterize switching in organic materials.[83] The sequential fabrication process is described in detail. A silicon oxide film with a thickness of 100 nm was deposited on a heavily doped p-type silicon substrate. Electron-beam lithography was used to define via-hole junctions with six different feature sizes: 40 μm, 8.5 μm, 4.5 μm, 1 μm, 500 nm, and 200 nm. To expose the bottom electrode, the silicon oxide film was etched using a 6:1 buffered oxide etchant. The via-holes were filled via polymer spin-coating. The chemical structure of the WPF-oxy-F polymer is shown schematically in **Figure 6**a. To create the top electrodes on the deposited polymer layer, an Ag layer with a thickness of 100 nm was deposited using a shadow mask. The fabricated organic memory device consisted of Ag/WPF-oxy-F/p$^+$ Si layers, as shown in Figure 6b. Current only flows through the via-hole junction. Figure 6c shows an AFM image of a via-hole device with an active area of 200 nm × 200 nm. Figure 6d shows a tilted scanning electron microscopy (SEM) image of the organic memory device. Representative bipolar switching in a via-hole device with an active area of 500 nm × 500 nm was obtained (Figure 6e), and this behavior was identical to that of devices with feature sizes of approximately 100 μm, suggesting the

© 2011 WILEY-VCH Verlag GmbH & Co. KGaA, Weinheim

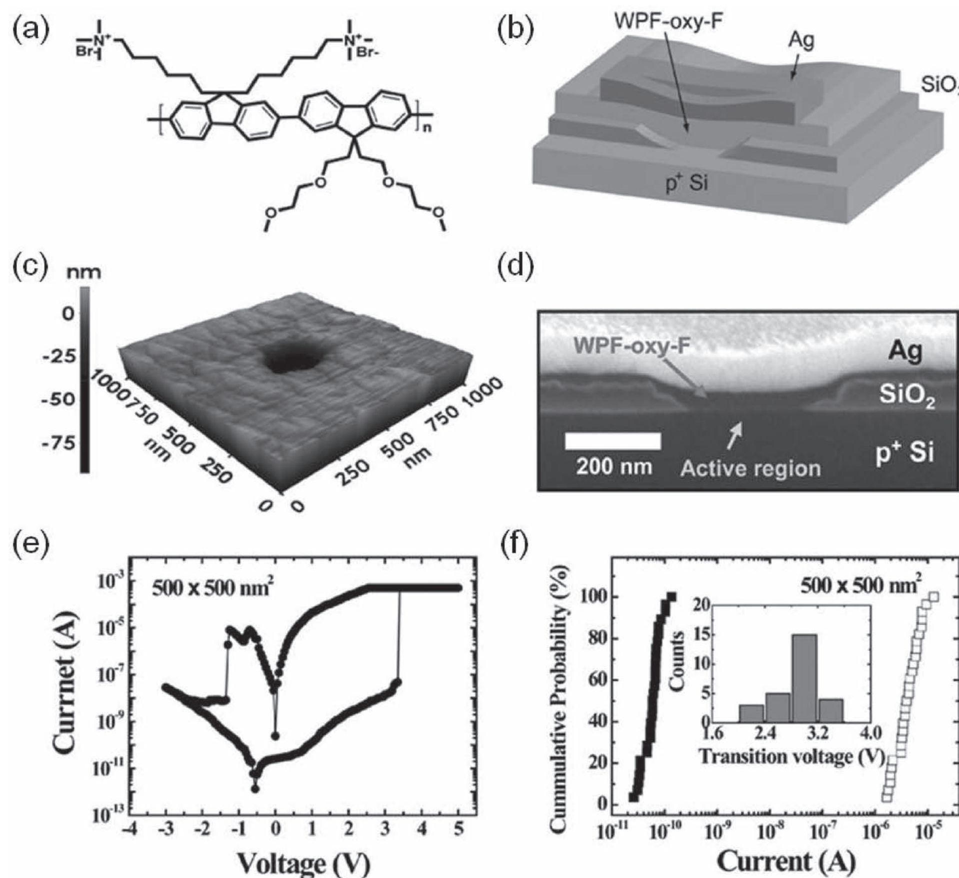

Figure 6. a) Chemical structure of WPF-oxy-F polyfluorene derivative. b) Schematic of a polymer memory device in a via-hole structure. c) AFM image of a via-hole of area 200 nm × 200 nm. d) SEM image of a tilt view of a via-hole polymer memory device. e) Semilog scale *I–V* characteristics of a polymer memory device with a 500 nm × 500 nm via-hole. f) Cumulative probability data set for polymer memory devices with a 500 nm × 500 nm via-hole (28 devices), showing a good device-to-device switching uniformity. The inset figure shows the histogram of the OFF-to-ON transitions for polymer memory devices with a 500 nm × 500 nm via-hole. Reproduced with permission.[83] Copyright 2009, IOP Publishing Ltd.

feasibility for submicron-scale organic memory applications. The basic operation of our memory device can be described by the SCLC model with filamentary conduction.[31] The statistical memory parameters (ON and OFF currents and transition voltages) were also narrowly distributed, indicating excellent switching uniformity (Figure 6f). These electrical characteristics suggest that the WPF-oxy-F polymer can be employed in high-density memory applications. In addition, the scalable via-hole structure can act as a useful test bed for evaluating the electrical characteristics of nanoscale organic devices.

As a more practical method to downscale cross-bar array organic memory devices, we used the direct metal transfer (DMT) method, a unique pattern transfer technique.[107] DMT is a nonaqueous process that is suitable for transferring metal patterns from a stamp directly onto a substrate at a low temperature and pressure (100 °C and 2 MPa). This method can also reduce damage to the organic layer and enable the three-dimensional stacking of device applications. The sequential process flow of the DMT method for cross-bar array memory devices with 2-μm feature sizes is illustrated in **Figure 7**. The first step is the preparation of a glass stamp, as shown in Figure 7a. A transparent glass stamp with a 2-μm line width was fabricated using conventional photolithography techniques. The surface of the glass stamp was treated with a monolayer of a releasing material, tridecafluoro-1,1,2,2-tetrahydrooctyltrichlorosilane,[108] and to easily detach the metallic layer from the glass stamp, an Au/Ag double layer (35 nm) was deposited on the releasing layer. The second step is the preparation of the bottom electrode and spin-coating of the polymer layer (Figure 7b). The bottom electrodes, with a 2-μm line width, were prepared on the silicon-on-insulator wafer using conventional lithography techniques. Heavily doped p-type polysilicon was used to pattern eight bottom electrode lines. The next step is the key process of the DMT method: transfer of the top electrodes onto the substrate (Figure 7c). The metal-deposited glass stamp was vertically aligned with the bottom electrodes and pressed at a temperature of 100 °C and a pressure of 550 psi for 10 min. After detaching the glass stamp from the polymer layer (Figure 7d), fabrication of the organic memory devices with an 8 × 8 cross-bar array and a junction area of 2 μm × 2 μm was completed. Lee et al.[109] also successfully fabricated nanoscale metal patterns for organic memory devices using the same technique. A DMT method featuring a two-step thermal treatment was capable of transferring metal lines with a 70-nm half-pitch

© 2011 WILEY-VCH Verlag GmbH & Co. KGaA, Weinheim

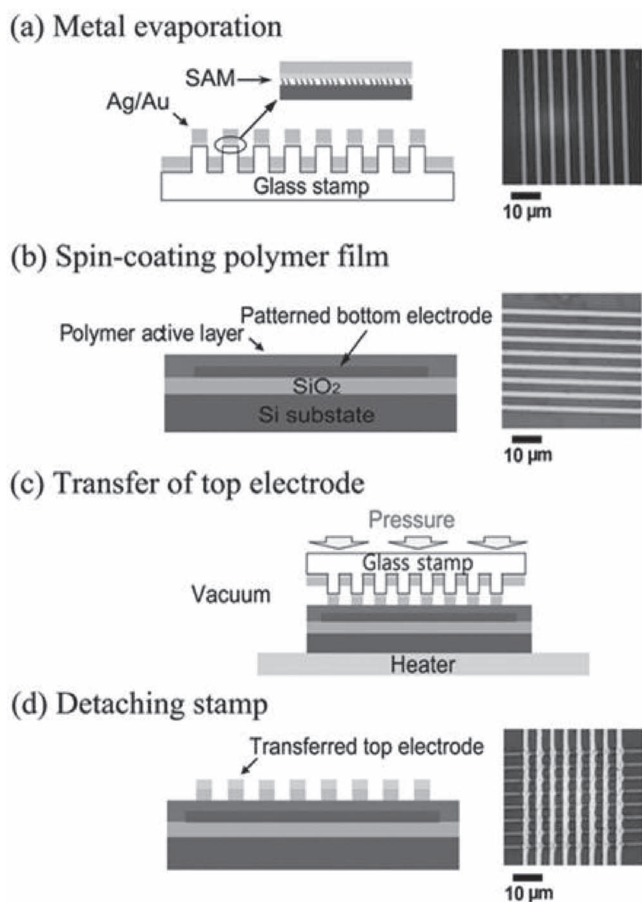

Figure 7. Fabrication process of cross-bar type polymer non-volatile memory devices using the DMT method. a) Metal evaporation on patterned glass stamp; b) spin-coating of polymer layer on the patterned bottom electrode; c) transfer of top electrode; d) detaching the stamp. Reproduced with permission.[107] Copyright 2008, IOP Publishing Ltd.

to an organic active layer. This unique strategy for producing high-density organic memory devices simplifies the fabrication process and lowers the costs of production.

Electrical switching in nanoscale junctions is often characterized with conducting atomic force microscopy (CAFM).[31,37] Lau et al.[37] developed a novel scanning probe technique to capture images of electrical responses in a Pt/stearic acid/Ti structure. The nanoscale conductance peaks of the scanned area appeared or disappeared depending on the conductance state. This result indicates that the formation and dissolution of individual nanoscale filaments caused conductance switching. The specialized CAFM technique can be used to assess nanoscale switching prior to the fabrication of nanoscale memory devices.

3.2.2. Multi-bit Storage Capability

Unlike complex concepts such as downscaling or multi-stacking, the multi-bit memory approach is a simple method for increasing integration density. A variable initial program voltage magnitude for conductance transition can provide access to multi-conductance states. The multi-conductance states of a variety of organic materials have been demonstrated.[36,38,63,91,110,111] In particular, multi-bit storage capabilities are commonly observed in unipolar switching including NDR region.[63,110,112] Reddy et al.[63] reported multilevel conductance switching in unipolar memory devices consisting of ITO/Tris(8-hydroxyquinolinato)aluminum (AlQ_3)/Al/Alq_3/Al. The intermediate states between the ON and OFF states were accessed by applying a voltage within the NDR region. The authors proposed that the field-induced transfer of charge carriers between AlQ_3 and the aluminum core was responsible for the observed conductance switching. Additionally, the multilevel conductance states remained constant during continuous stress tests, indicating the stability of both the material and the material-electrode interfaces. A similar multilevel memory effect has also been demonstrated in inorganic SiO thin-film structures.[112] A detailed experimental study revealed that filament formation was the dominant mechanism in switching from the OFF state to the lower ON state[94], while the Poole-Frenkel effect dominated switching from the lower ON state to the higher ON state.[113,114] Das et al.[38] examined voltage-driven electrical multilevel in the bipolar switching of an organic semiconductor, namely Ponceau SS. Typical bipolar I–V curves of Ponceau SS sandwiched between ITO and Al electrodes are shown in **Figure 8**a. Variable high-conducting states were formed, depending on the magnitude of V_{Max} (Figure 8b). The authors reported that this might be attributed to the switching of a higher number of molecules upon application of a higher voltage amplitude or the presence of more than one stable conducting conformer in the molecules. To demonstrate multilevel memory, different pump voltages (±1.8, ±2.2, and ±2.6 V) were applied, and the current states were probed as a function of time (Figure 8c). A write-read-erase-read voltage pulse sequence for multilevel memory is shown in Figure 8d. After write pulses of 1.8, 2.2 and 2.6 V or an erase pulse of –2.6 V was applied to the device, a read voltage pulse of 0.8 V was selected. The device showed four distinct current states ((0,0), (01), (10), and (11)), indicating two-bit memory. The results demonstrate the ability to achieve multilevel memory elements at the molecular scale.

NDR and multilevel memory effects were also obtained in organic devices consisting of an anthracene derivative, 9,10-bis-(9,9-di-(4-(phenyl-p-tolyl-amino)-phenyl)-9H-fluoren-2-yl)-anthracene (DAFA), sandwiched between Ag and ITO electrodes.[111] Different negative voltages produced multiple conductance states. To explain the NDR and multilevel effects, the charge trapping mechanism at the DAFA/Ag interface, which was caused by the diffusion of Ag atoms into the DAFA during the deposition process, was proposed. Mukherjee et al.[91] reported that multilevel conductance states could be created in Langmuir–Blodgett films of the organic semiconductor 2,3-dichloro-5,6-dicyano-1,4-benzoquinone (DDQ). The multilevel conductivity occurred as a result of density differences between the reduced DDQ molecules and the neutral molecules. The multilevel memory capabilities of an organic device containing 2-(hexahydropyrimidin-2-ylidene)-malononitrile (HPYM) molecules between Al/Al_2O_3 and Ag have also been observed.[36] The high conduction mechanism was governed by trap- and space-charge-limited conduction[85], and the low conduction mechanism was partially explained by the Poole–Frenkel emission model.[115] The existence of multilevel conductance states in this memory structure could be due to the different degrees of

© 2011 WILEY-VCH Verlag GmbH & Co. KGaA, Weinheim

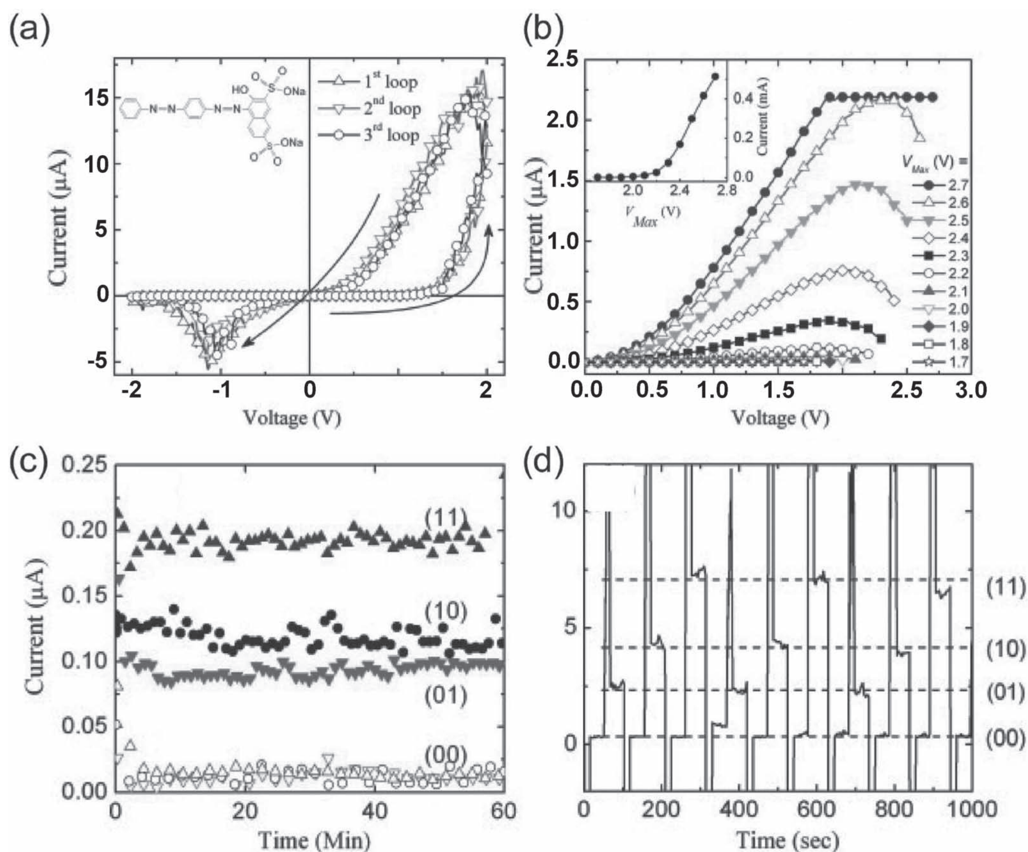

Figure 8. a) *I–V* characteristics of a device based on spun-cast film of Ponceau SS in three loops. Inset shows the molecular structure of a Ponceau SS molecule. b) *I–V* characteristics of a device based on spun-cast film of Ponceau SS from different values of $+V_{Max}$. For $V_{Max} = 2.7$ V, the current value reached the limit of the measuring instrument during the voltage sweep. Inset shows the current at 0.8 V as a function of V_{Max}. c) Multilevel read-only memory of a device based on spun-cast film of Ponceau SS. Current was read under a +0.8 V pulse (width 2 s; duty cycle = 17%); for (11), current values were divided by six for comparison. d) Multilevel random-access memory application of the same device. Current under ''write-read-erase-read'' voltage sequence is presented. Reproduced with permission.[38] Copyright 2008, Elsevier.

rearrangement of dipolar molecules. Various operating mechanisms have been proposed to explain the origin of the multiple observed states. However, the absence of an established model or theory related to these phenomena has hindered the implementation of multiple stable conductance states. Thus, the operation mechanisms of multi-bit memory should be further studied.

3.3. Architectural Concepts for Advanced Memory Devices

3.3.1. Active Matrix Systems: 1T-1R and 1D-1R

The cross-talk phenomenon in memory cells often occurs due to parasitic leakage paths (called sneak paths) through neighboring cells with low resistances in cross-bar array structures[66,68] or the presence of excess currents that can cause electrical damage.[116] These phenomena disturb the reading process in selected cells, which must be eliminated in practical memory applications. To solve the cross-talk problem, a switching element (diode or transistor) can be added to each memory cell.[117] The International Technology Roadmap for Semiconductors[118] has also stressed the incorporation of switching elements in cross-bar array memory structures. Indeed, the one diode and one resistor (1D-1R)[119,120] or one transistor and one resistor (1T-1R)[121] architectures improve reading accessibility without disturbing the reading process.

Array circuits with the 1T-1R and 1D-1R architectures have been demonstrated with complementary metal-oxide-semiconductor (CMOS) technologies to study inorganic-based memory devices.[66,116,122] The Samsung Advanced Institute of Technology is one of the leading groups in this research field. Lee et al.[66] reported the combination of a Pt/NiO/Pt memory element with nonvolatile resistance switching behavior and a $Pr/VO_2/Pt$ switching element with threshold resistance switching behavior. The main advantages of such a memory structure include an extremely fast switching speed of several tens of nanoseconds and a low processing temperature below 300 °C, which is suitable for three-dimensional structures. High-performance oxide-based nonvolatile memory devices were also investigated by Ahn et al.[120] A p–n CuO/$InZnO_x$ diode was used as a switching element, and Al_2O_3 anti-fuse was used as a storage node. The memory cells showed large ON/OFF ratios of approximately 10^6, small current distributions at programmed and unprogrammed states, and a fast switching

© 2011 WILEY-VCH Verlag GmbH & Co. KGaA, Weinheim

speed of approximately 20 ns. They also demonstrated the applicability of the advanced memory architecture using a select transistor (GIZO-based transistor) in a peripheral circuit with an existing all-oxide 1D-1R structure.[123] The individual components exhibited the required material properties: bistable storage node, rectifying diode, and select transistor.

Active matrix systems (1D-1R or 1T-1R) in organic electronics are also necessary for practical memory applications. Möller et al. reported an architecture for WORM memory based on the hybrid integration of an electrochromic conducting polymer with a thin-film silicon p–i–n diode.[62] This work was the first demonstration of the integration of both organic memory and switching components into a single chip. The platform not only prevents reading disturbance but also potentially enables high-density memory applications with vertical stacking structures. Our group has also made progress in the development of this hybrid structure. We demonstrated a hybrid-type 1T-1R circuit consisting of an inorganic transistor (p-MOSFET) and a polymer memory.[121] **Figure 9**a shows a schematic and optical image of 1T-1R devices fabricated on a silicon substrate. Figure 9b shows the schematic of a one-bit 1T-1R cell and the chemical structure of the organic memory material (WPF-oxy-F). The p-MOSFET device was fabricated using a conventional CMOS process. An organic non-volatile memory device with cross-point architecture was fabricated on the drain side (p^+ Si) of the Si transistor, which was used as the bottom electrode (Figure 9b). When the switching component (p-MOSFET) was turned ON, the current flow from the source to the drain was modulated by the resistance state of the organic memory (Figure 9c).

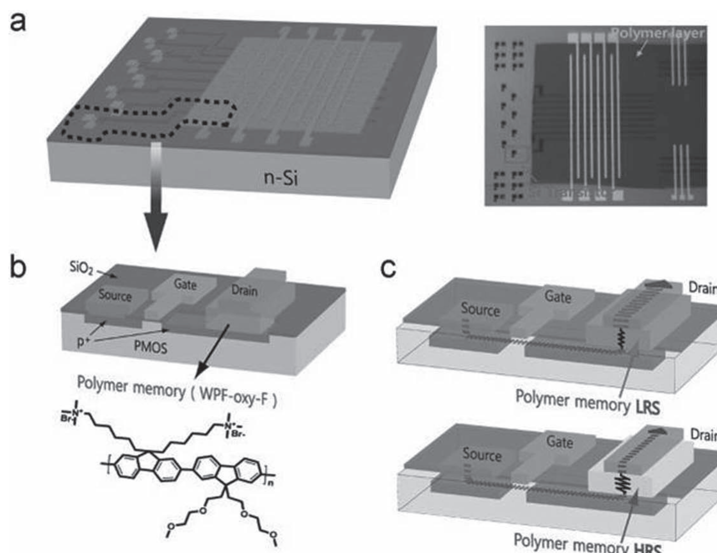

Figure 9. a) Schematic and optical image of 1T-1R hybrid devices. The area with the black dotted line indicates a silicon transistor (1T) and a polymer memory (1R). b) Schematic of a single 1T-1R device and chemical structure of WPF-oxy-F. c) Schematic of the basic operation of the 1T-1R device. The current flow from source to drain in the 1T-1R device is controlled by the resistance state of the polymer memory device (see text). Reproduced with permission.[121]

We also performed $I–V$ characterizations of the p-MOSFET and organic memory devices. **Figure 10**a shows the drain current versus drain voltage ($I_D–V_D$) characteristic of the p-MOSFET device and its circuit diagram (inset). To turn the p-MOSFET device ON, we applied a negative bias to the gate electrode. The drain current was saturated at approximately –70 μA at a gate bias of –2 V, indicating typical long channel p-MOSFET behavior. The organic memory devices showed typical bipolar switching behavior (Figure 10b). The polymer memory device exhibited turn-ON and turn-OFF events at 3 V and –2 V, respectively. To evaluate the $I–V$ characteristics of the p-MOSFET combined with the organic memory, we measured the $I_D–V_D$ and drain current versus gate voltage (I_D-V_G) characteristics of the 1T-1R device. As shown in Figure 10c, when the organic memory device was in the LRS condition, the 1T-1R device showed a $I_D–V_D$ curve similar to that of the p-MOSFET device alone. This result indicates that the memory component in the LRS condition did not affect the operation of the transistor. However, because of the series resistance of both the channel and the polymer memory, the current level in the saturation regime of the 1T-1R device (Figure 10c) was reduced by a factor of 0.7 compared to the single transistor under the same gate bias. In contrast, when the organic memory device was programmed to the HRS, the current flow from the source to the drain in the p-MOSFET device was significantly interrupted by the high resistance of the organic memory device. In the HRS condition, a low current of approximately 10 nA flowed from the source to the drain through the 1T-1R device under a gate bias of –2 V. The drain current for the 1T-1R device at a fixed drain bias of –0.1 V was 10 μA (in the LRS condition) and 10 nA (in the HRS condition) (Figure 10d). This result indicates that the drain current of the 1T-1R device could be controlled by the resistance states of the organic memory device. Thus, we successfully demonstrated the performance of 1T-1R hybrid-type memory devices.

Compared to the integration of the 1T-1R structure, the 1D-1R architecture is preferred because it occupies less area, approximately $4F^2$, where F is a minimum feature size. Furthermore, the design and fabrication are simpler for 1D-1R circuits than for 1T-1R devices. For these reasons, 1D-1R systems, such as WORM memory devices combined with a diode[119] and a diode-switch organic nonvolatile bistable memory,[67] have recently been developed. However, the electrically irreversible switching of these devices limits their application in situations in which a rewritable capability is required. Electrically rewritable switching in the 1D-1R structure can be achieved only with the use of unipolar-type switching memory.[66–68] Meanwhile, the poor reliability and performance of organic diodes can prevent the 1D-1R system from operating ideally. Thus, we developed a hybrid-type 1D-1R structure combining an inorganic diode with organic unipolar memory.[65] **Figure 11**a shows a three-dimensional schematic of the 1D-1R devices with 16 unit

© 2011 WILEY-VCH Verlag GmbH & Co. KGaA, Weinheim

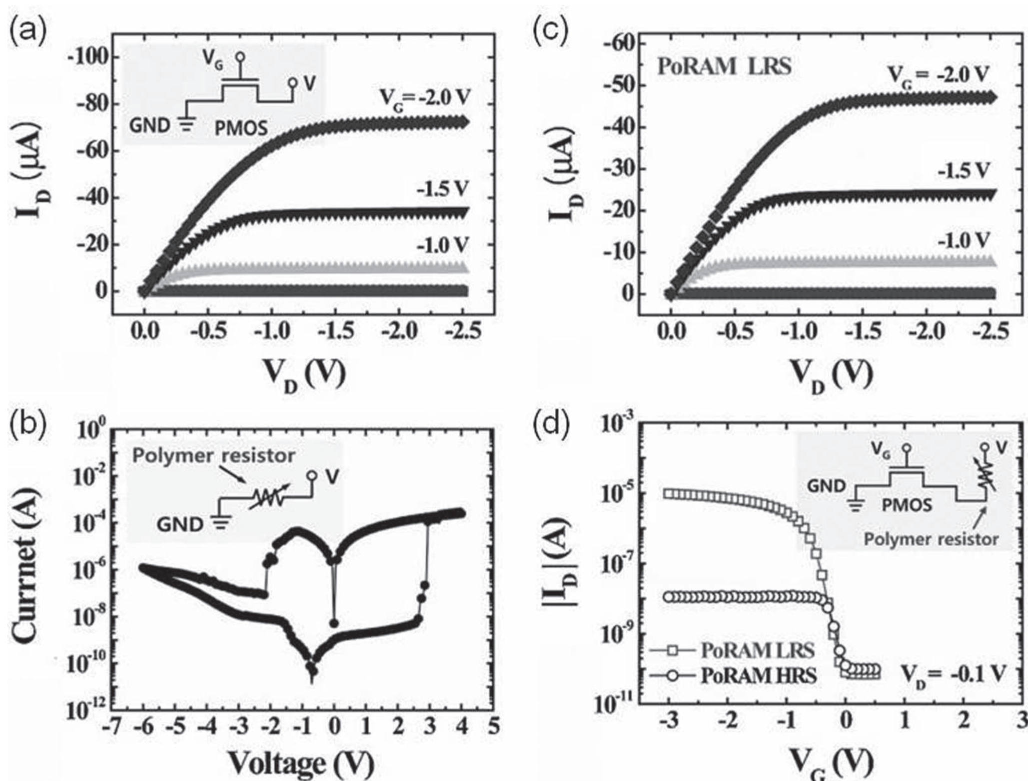

Figure 10. a) I_D–V_D characteristics of the p-MOSFET device and its circuit diagram. b) *I–V* characteristics of polymer memory device and its circuit diagram. c) I_D–V_D characteristics of the 1T-1R device. d) I_D–V_G characteristics of the 1T-1R device with respect to the resistance state of the polymer memory device. Reproduced with permission.[121]

cells. A cross-sectional image and electronic circuit diagram of the device are illustrated in Figure 11b. In the 1D-1R devices, an inorganic Schottky diode was created at the Schottky junction between the Al and p-type Si. The organic resistive memory component consisted of a PI:PCBM composite sandwiched between Al and Au electrodes. The *I–V* characteristics of the inorganic Schottky diode and organic resistive memory were tested and found to be asymmetrical (Figure 11c). Figure 11d shows the typical unipolar switching *I–V* curves of an organic resistive memory device. A 1D-1R device with bipolar memory is not erasable due to the suppressed current at the reverse polarity. Instead, unipolar memory is required to implement the electrically rewritable switching of 1D-1R devices. Figure 11e shows the *I–V* characteristic of a 1D-1R memory cell (p-Si/Al/PI:PCBM/Au). Unipolar switching characteristics were observed in the forward bias regime, while switching in the reverse bias regime disappeared due to the rectifying property. The ON/OFF ratios for 1R and 1D-1R devices as functions of the applied voltage were compared (Figure 11f). The ON/OFF ratio of the 1R device was constant regardless of the voltage polarity because of the symmetrical *I–V* behavior of this device. However, the ON/OFF ratios of the 1D-1R devices were completely different depending on the voltage polarity, and this result was attributed to the diode component.

Unnecessary leakage paths in cross-bar array structures can form through the neighbors of a selected cell if the polymers lack rectification properties.[66,68] These paths affect the reading process and cause misreading errors (i.e., they produce cross-talk phenomena). We experimentally observed such reading disturbances in 1R array-type memory devices (**Figure 12**a,b). Specifically, if cells (1,2), (2,1), and (2,2) were set to the ON states and the (1,1) cell was initially set to the OFF state, the (1,1) cell was read as possessing an ON resistance (7.9 kΩ) as a result of the leakage path (2,1) → (2,2) → (1,2). This indicates that the selected OFF state could be misread as an ON signal. This reading disturbance problem can be prevented by adding diode components. If rectifying diode components are integrated into the resistive memory cells, the unintentional leakage path through the (2,2) cell can be prevented, and misreading can be avoided. To prove this, we tested a 2 × 2 array device consisting of 1D-1R cells. As illustrated in Figure 12c and d, when the ON state was set in neighboring cells (i.e., the (1,2), (2,1), and (2,2) cells), the OFF signal of the selected (1,1) cell was successfully identified without any reading disturbance. This improved reading capability can enable the production of high-density organic memory devices integrated with an array architecture. This research was the first demonstration of rewritable switching in organic-based 1D-1R systems. Nevertheless, a "realistic" active matrix system integrated with a cross-bar array structure requires new 1D-1R circuit designs and an improved device performance.

The development of a single element that simultaneously exhibits both switching and diode behavior could be the ultimate solution for the creation of matrix array structures

© 2011 WILEY-VCH Verlag GmbH & Co. KGaA, Weinheim

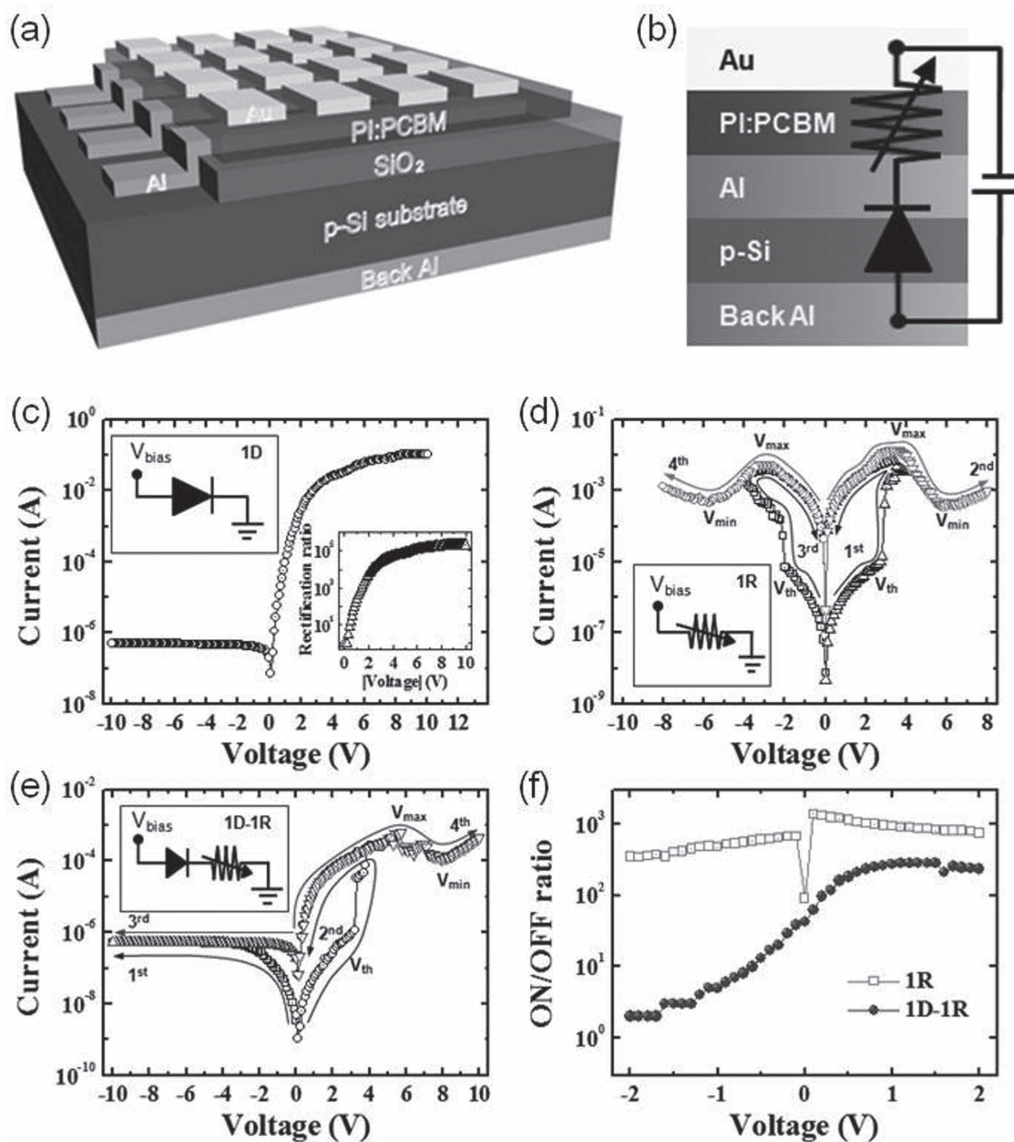

Figure 11. a) A schematic of a 1D-1R hybrid-type memory device. b) A schematic of the layered structure and an electronic circuit diagram of the 1D-1R device. c) *I–V* characteristics and circuit diagram (left inset) of an inorganic Schottky diode. Right inset shows the rectification ratio as a function of voltage. d) *I–V* characteristics of an organic resistive memory and its circuit diagram (inset). V_{th}, V_{max}, and V_{min} indicate the threshold voltage, the voltage at the local current maximum point, and the voltage at the local current minimum point, respectively. e) *I–V* characteristics and circuit diagram (inset) of a 1D-1R memory device. f) Comparison of the ON/OFF ratios for 1R and 1D-1R devices as a function of the applied voltage. Reproduced with permission.[65]

because its cell structure and fabrication process would be simpler than those of common 1D-1R structures with two elements.[34,50,124] For instance, a single device consisting of ITO/PEDOT:PSS:NaCl/6T-PEO block copolymer/Al showed resistive switching behaviors with rectifying properties.[50] The asymmetric response to bias polarity was attributed to selectivity in the transport of ions by the block copolymer. Similarly, Asadi et al.[34] developed a single storage medium consisting of a phase-separated blend of organic ferroelectric and semiconducting polymers that produced bistable rectifying diodes. Recently, these authors designed and performed an extended experiment.[124] They used the previously developed phase-separated blend of ferroelectric (star-shaped matrix) and semiconducting polymers (spheres) (**Figure 13**a). The polarization field of the ferroelectric polymer modulated the injection barrier at the semiconductor contact.[34] The diodes could be switched at biases larger than the coercive field (Figure 13b). Both symmetric and rectifying *I–V* curves were observed with current modulations of up to 10^6. To further demonstrate the feasibility of the ferroelectric diodes, 9-bit memory cells in a $4F^2$ cell configuration were fabricated (Figure 13c). The most difficult state, the state that is the most sensitive to cross-talk, was created as shown in Figure 13d. A single low-conducting "0" bit was in the center of the 3×3 array, and it was surrounded

© 2011 WILEY-VCH Verlag GmbH & Co. KGaA, Weinheim

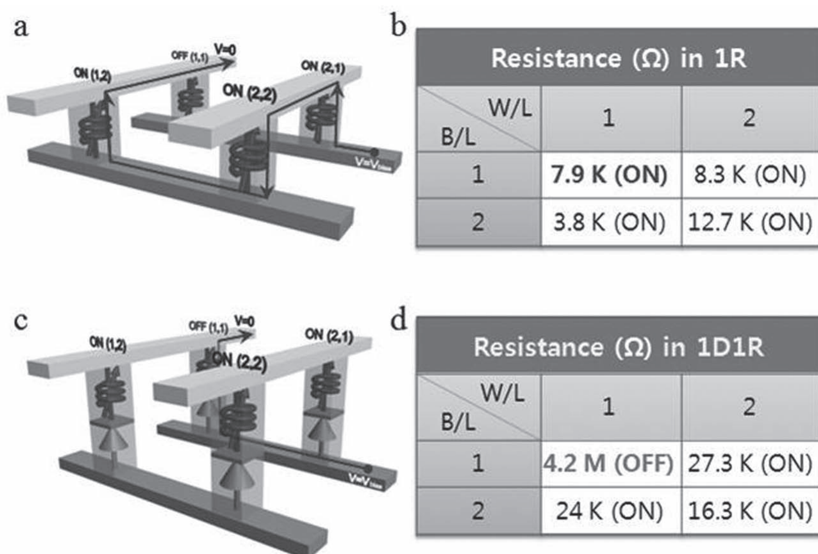

Resistance (Ω) in 1R

B/L \ W/L	1	2
1	**7.9 K (ON)**	8.3 K (ON)
2	3.8 K (ON)	12.7 K (ON)

Resistance (Ω) in 1D1R

B/L \ W/L	1	2
1	4.2 M (OFF)	27.3 K (ON)
2	24 K (ON)	16.3 K (ON)

Figure 12. The reading process of the 1R array type memory device. a) Schematic illustration of cross-talk interference during the reading of an OFF (1,1) cell when neighboring cells ((1,2), (2,1), and (2,2)) were set to the ON state. b) Resistance values of each cell in the 1R device. Each resistance was measured at a voltage of 1 V. The (1,1) cell was misread as an ON signal due to interference from neighboring cells during reading. The reading process of the 1D-1R array type memory device. c) Schematic illustrating current flow during the reading of an OFF (1,1) cell when neighboring cells ((1,2), (2,1), and (2,2)) were set to the ON state. d) Resistance values of each cell in the 1D-1R device. Each resistance was measured at a voltage of 1 V. The (1,1) cell was accurately read as an OFF signal, demonstrating the absence of the cross-talk problem. Reproduced with permission.[65]

by 8 high-conducting "1" bits. The most challenging state, 111101111, was unambiguously identified without cross-talk (Figure 13e). Cross-talk in a cross-bar geometry was prevented by the rectifying properties of the phase-separated blend. This result indicates a step toward immortal memory, a cross-talk-free memory array with an unpatterned storage medium.

3.3.2. Flexible Memory Applications

Flexibility is required for future electronic applications, such as foldable and stretchable electronics. A variety of technologies have been conceived and applied to achieve flexibility in organic and inorganic electronics, and new concepts are being developed. In particular, the evolution of flexible electronic applications that require information storage components has advanced research on flexible memory devices.[6,53,69,125–128] A method for depositing inorganic-based switching materials onto flexible polymer substrates has been suggested as a promising approach for flexible memory applications.[6,125,126] Thus, low-temperature processing techniques are required to prevent polymer-based flexible substrates from being transformed during the fabrication process. Kim et al.[125] treated Al films with plasma oxidation to form aluminum oxide, which is an active switching material for nonvolatile memory applications. The high ductility of the Al films provides excellent flexibility. Furthermore, the low-temperature plasma oxidation process is advantageous for producing flexible electronic devices. Flexible TiO_2 cross-bar array devices on plastic substrates were successfully demonstrated using a low-temperature (80 °C) process; the devices showed stable endurance and low switching

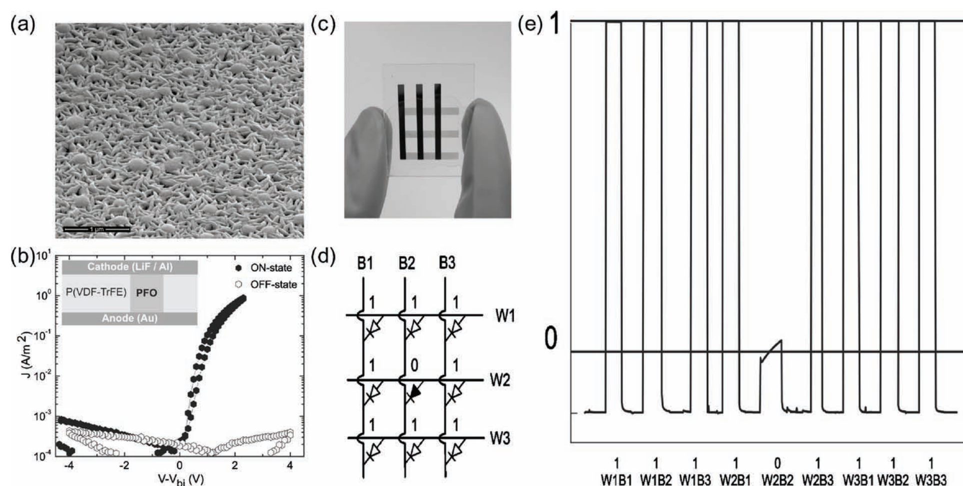

Figure 13. a) SEM micrograph of the phase-separated morphology and b) *J–V* characteristics of a bistable rectifying diode based on a phase-separated 10/90 wt% blend of a ferroelectric polymer, P(VDF-TrFE), and a semiconducting polymer, PFO. The SEM image was captured at a tilt angle of 52°. The diode was fabricated with a gold bottom electrode and an LiF/Al top electrode. The total device area was 1 mm^2. The diode was poled with pulses of +/−20 V, exceeding the coercive field. The voltage axis was corrected for the built-in voltage of approximately 1.5 V. The inset in b) shows the device layout. c) A photograph of a 3 × 3 cross-bar memory array. The width of the electrode line and spacing were approximately 3 mm. d) Equivalent circuit of the 3 × 3 array shown in (a) programmed with the 111101111 logic state. e) The current passing through each individual bit in the 111101111 logic state over time. The measurement shows that cross-talk was eliminated; the programmed state was nondestructively read. Reproduced with permission.[124] Copyright 2010, American Institute of Physics.

© 2011 WILEY-VCH Verlag GmbH & Co. KGaA, Weinheim

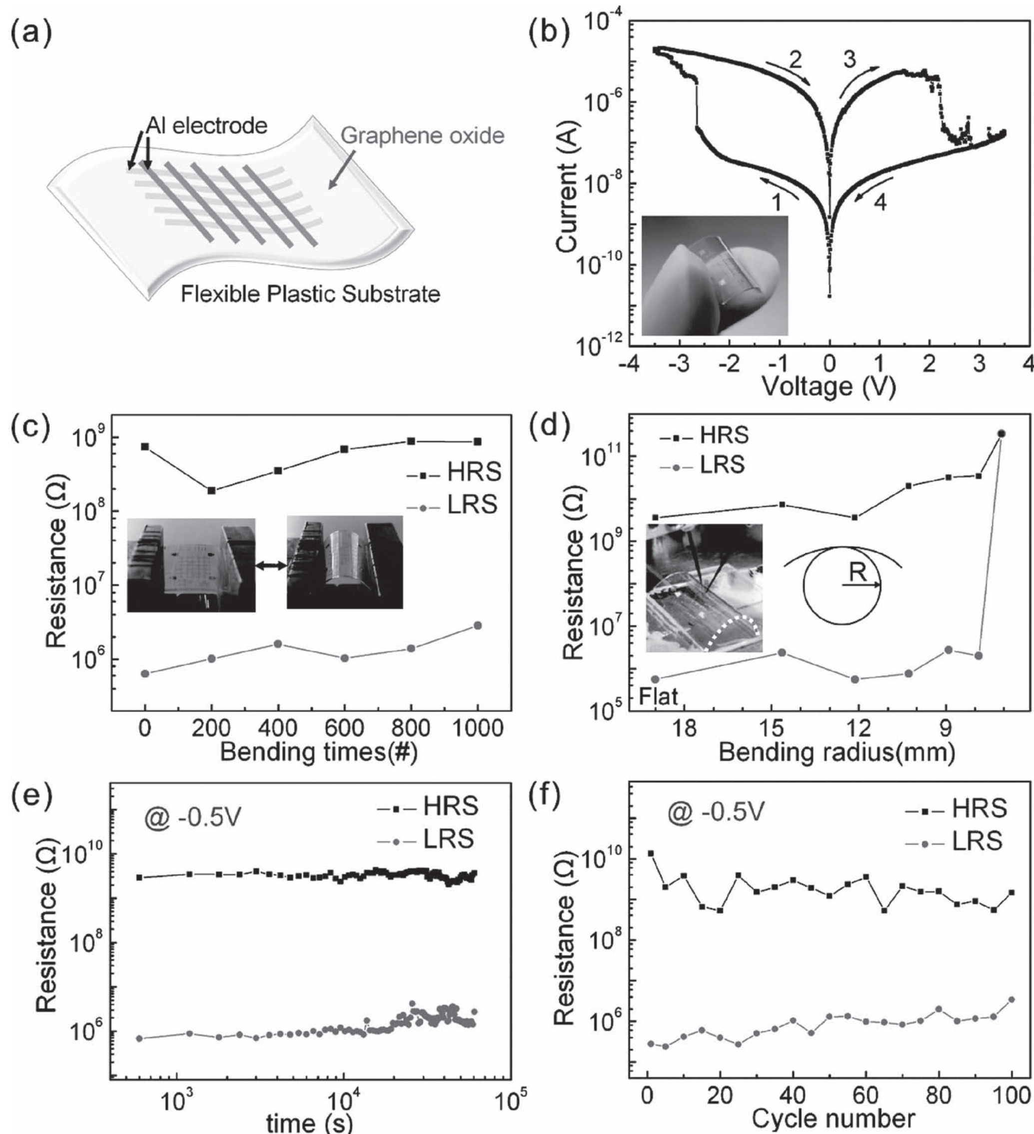

Figure 14. a) A schematic illustration of a G-O based flexible cross-bar memory device. b) Typical *I–V* curve of an Al/G-O/Al/PES device plotted on a semilogarithmic scale. The arrows indicate the voltage sweep direction. The left inset is a real photo image of a device. c) Continuous bending effect of an Al/G-O/Al/PES device. The insets show photographs of repeated two bending states. d) Resistance ratio between the HRS and LRS as a function of the bending radius (R). The inset is a photograph of an I–V measurement being performed under a flexed condition. e) Retention test of an Al/G-O/Al/PES device read at –0.5 V. (f) Endurance performance of an Al/G-O/Al/PES device measured over 100 sweep cycles. Reproduced with permission.[127] Copyright 2010, American Chemical Society.

voltages comparable to those observed in memory cells on rigid substrates.[6] Multi-stacked memory architectures could also be readily constructed by a simple additional process. Furthermore, mechanical robustness without interlayer cell-to-cell interference was achieved. The structural and electrical properties of flexible substrates should be considered when attempting to produce reliable switching properties. In place of common polymer substrates, such as polyethylene–terephthalate and polyethylene–naphthalate, stainless steel could be used as an alternative flexible substrate because it has a high corrosion resistance, high conductivity, and thermal stability.[129] For these reasons, the stainless steel substrate demonstrated excellent flexibility in a ZnO-based RRAM.[126] The ZnO-based flexible memory devices exhibited stable and reliable resistive switching behaviors over 100 switching cycles and were not degraded upon bending. These results indicate that stainless steel could be used as both a substrate and an electrode in flexible RRAM applications.

Although metal-oxide-based resistive memory devices have several advantages, such as scalability, low power consumption, and fast switching speeds, their use with large-area flexible substrates has been limited because of their material characteristics and high-temperature fabrication process. As a promising nonvolatile memory technology, Jeong et

© 2011 WILEY-VCH Verlag GmbH & Co. KGaA, Weinheim

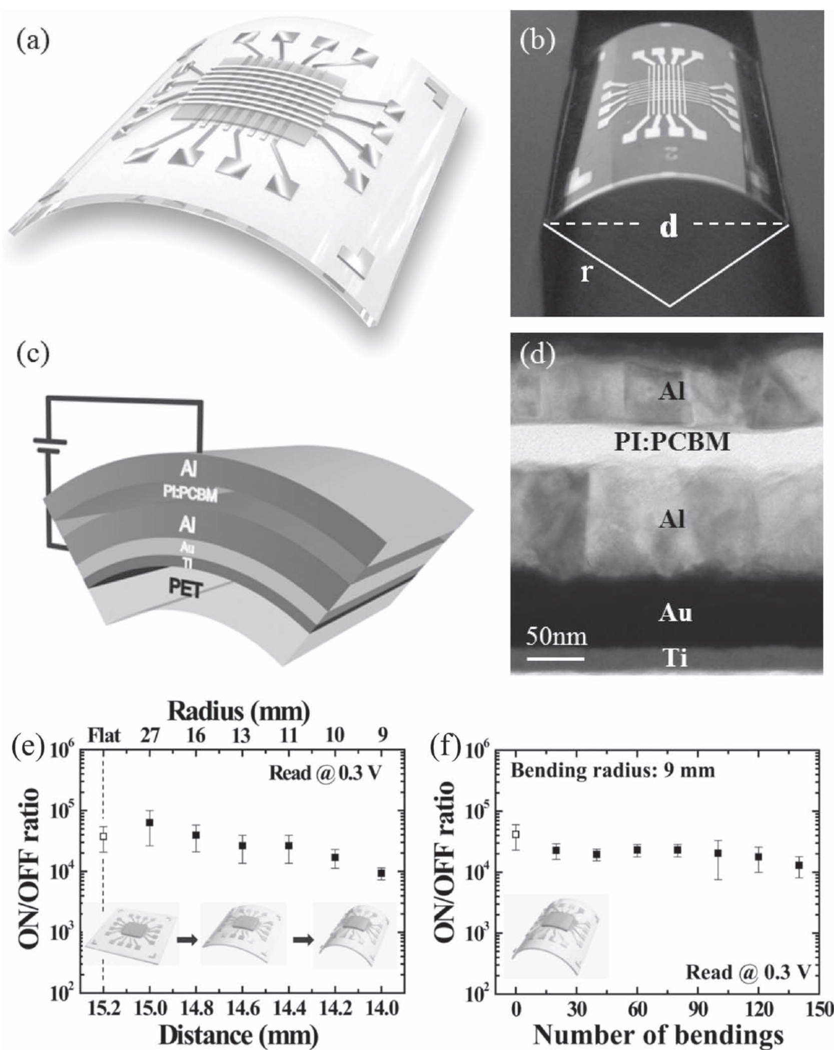

Figure 15. a) Illustrated and b) optical images of a Ti/Au/Al/PI:PCBM/Al flexible organic memory device in an 8 × 8 array. c) Schematic view of a Ti/Au/Al/PI:PCBM/Al memory cell. d) Cross-sectional TEM image of the layers in a memory cell. e) On/off ratio as a function of the bending condition (the substrate distance and the bending radius). f) On/off ratio as a function of the number of bendings. Reproduced with permission.[128]

al.[127] developed a memory device based on graphene-oxide (G-O) using a simple spin-coating method on a flexible substrate. This device showed a reliable memory performance. A 5 × 5 cross-bar memory structure with G-O films sandwiched between Al electrodes on a flexible polyethersulfone (PES) substrate is shown in **Figure 14**a. The Al/G-O/Al/PES flexible device showed bipolar resistive switching behaviors (Figure 14b). The authors proposed that the bipolar switching in such Al/G-O film/Al devices could be associated with the formation and rupture of conducting filaments in the insulating barrier at the top interface and not throughout the entire G-O bulk film.[130,131] To confirm the feasibility of the G-O device for flexible memory applications, mechanical flexibility tests were performed. During the large number of bending tests, which included 1000 cycles, the switching properties were not degraded; the devices maintained an ON/OFF ratio of greater than 10^2 (Figure 14c). Figure 14d shows the results of a bending test as a function of bending radius (R). The ON/OFF ratio of the flexible memory device remained constant without any serious degradation, even in the maximum bending condition with a 7-mm bending radius. This was a result of the excellent mechanical properties of the G-O film, which was stable even in an extremely flexed state. The memory performance of this device, in terms of retention and endurance, was also evaluated. Figure 14e shows the retention behavior of the G-O film flexible memory device. Two resistance states were maintained for approximately 10^5 sec without serious changes. The endurance stability was also assessed, and operation was steady for over 100 cycles (Figure 14f). This research is an important step toward the application of G-O films in flexible memory electronics.

Indeed, the use of flexible memories based on organic materials is important because of their simplicity, low manufacturing costs, and flexibility. Several studies on organic memory devices fabricated on flexible substrates have been conducted.[53,69,128,132] Using organic transistors with a floating gate embedded in hybrid dielectrics with a 2-nm SAM and a 4-nm plasma-grown metal oxide, Sekitani et al.[132] produced transistor-type memory arrays on flexible plastic substrates. The transistors endured more than 1000 program and erase cycles. By integrating a flexible array of organic floating-gate transistors with a pressure-sensitive rubber sheet, these authors demonstrated a sensor matrix capable of detecting the spatial distribution of applied mechanical pressures and storing the analog sensor input as a two-dimensional image over long periods.

Printable organic materials are one of the most important emerging technologies for the mass production of large flexible electronics. These technologies have been used in two-terminal-based organic resistive memory devices. A printed cross-bar Cu/CuPc/PEDOT:PSS/Ag system was applied to a flexible polyester substrate, and bistable switching behavior was observed.[133] Printability is necessary for item-level RFID tags, large-area sensors, flexible displays, and many other emerging electronic applications. Conductive polymer films[134,135] can further improve the bending stability of flexible electronics. Conductive polymer electrodes have been used for a flexible polymer memory device in a sandwich structure containing a polypyrrole (PPy)/conjugated copolymer of 9,9-dihexylfluorene and benzoate with a chelated europium-thenoyltrifluoroacetone ligand complex/Au.[69] The conducting PPy film acted as both the conductive electrode and the flexible substrate. With flexible and conductive PPy substrates, polymer memory could meet future demands for data storage.

 © 2011 WILEY-VCH Verlag GmbH & Co. KGaA, Weinheim

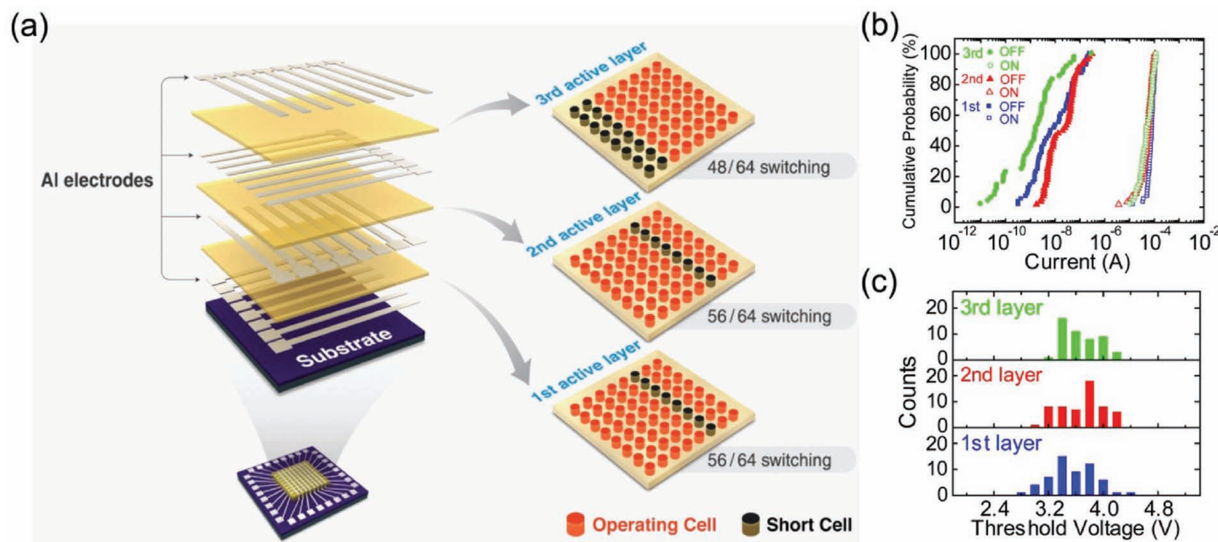

Figure 16. a) Illustration of the 3D-stacked memory assembly (left) and statistical distribution of the memory-operative cells (red) and the electrically shorted cells (black) in each active layer (right). b) Cumulative probability data for all operative cells (160 operative cells out of 192 fabricated cells). c) Statistical distribution of the threshold voltages of the operative cells in each active layer. Reproduced with permission.[136]

Recently, our group reported the excellent bending stability of an organic memory device with an 8 × 8 cross-bar array on a flexible substrate, as shown in **Figure 15**a.[128] Figure 15b shows an image of a fabricated memory device under bending. Figure 15c illustrates a schematic cross-sectional view of the structure of the Ti/Au/Al/PI:PCBM/Al layers on the flexible polymer substrate. We used the Ti/Au bilayer (Ti as an adhesion layer and Au as a buffer layer) to minimize the oxidation of the bottom Al electrodes. Figure 15d shows a cross-sectional TEM image of the memory cell. The TEM results show no agglomerations of PCBM, indicating the uniform dispersion of PCBM in PI. Electrical stability under severe bending is a key requirement for flexible memory devices. Thus, we investigated the ON/OFF ratio as a function of the degree of bending. As shown in Figure 15e, the ON/OFF ratios of the memory device were maintained at 10^4 even in the maximum bending condition with a 14-mm bending radius. In addition, the memory performance was stable under repetitive bending cycles, as shown in Figure 15f. The device maintained an ON/OFF ratio of over 10^4 without any significant electrical degradation over 140 cycles. These results indicate that our memory device could be promising for future flexible memory devices.

3.3.3. Three-Dimensional Integration

Vertically stacked three-dimensional architectures can greatly increase memory cell density.[6,70,136–139] Unlike inorganic-oxide-based memory devices, organic-layer devices can degrade during subsequent spin-coating processes, and thus, creating multiple vertically stacked layers in organic devices is not easy. To a certain extent, the success of multi-layer stacked device fabrication depends on either the chemical and thermal robustness of organic materials or the deposition method. For instance, the material methyl-silsesquioxane (MSQ) has good planarization properties and excellent chemical stability so that nanoimproint lithography was applied for downscaling and cross-bar array memory devices with cell size of 100 nm scale were also three-dimensionally stacked.[139] Furthermore, silver-doped MSQ was found to exhibit excellent memory performance.[139] Kwan et al.[137,138] reported a stackable organic memory device that used a photo-cross-linkable copolymer. The multi-stacking process was possible because the polymer film, once cross-linked, could resist high temperatures and was sufficiently robust to withstand lithography processes. This material could also be at once patterned using a photomask, thus reducing the number of processing steps. The Multi-layer stackable polymer memory devices offer a promising new direction for hybrid polymer-CMOS applications.

Recently, we also developed a polymer resistive memory device with a three-dimensional stacked 8 × 8 cross-bar array, based on a composite of PI and PCBM.[136] Simple spin-coating processes were used to stack the active polymer layers. Once the composite layer was cured at a high temperature, the following spin-coating process was performed easily due to the thermal and chemical robustness of the PI film. **Figure 16** shows statistical data for the fabricated memory cells in the three active layers. Both operative and inoperative cells are distinguished with each different color. The left images in Figure 16a show the three organic memory layers sandwiched between Al electrode layers, while the right images show how the operative and inoperative cells (electrical short cells) were distributed in each layer. Despite losses in some cells, the memory assembly produced a high yield: 87.5% in the first and second active layers and 75% in the third layer. This result indicates that three-dimensionally stacked multilayer cross-bar organic memory arrays are possible and that the introduction of additional organic layers can enable the high-density integration of organic memory devices. The cumulative probability of obtaining the ON and OFF currents in all operative memory

© 2011 WILEY-VCH Verlag GmbH & Co. KGaA, Weinheim

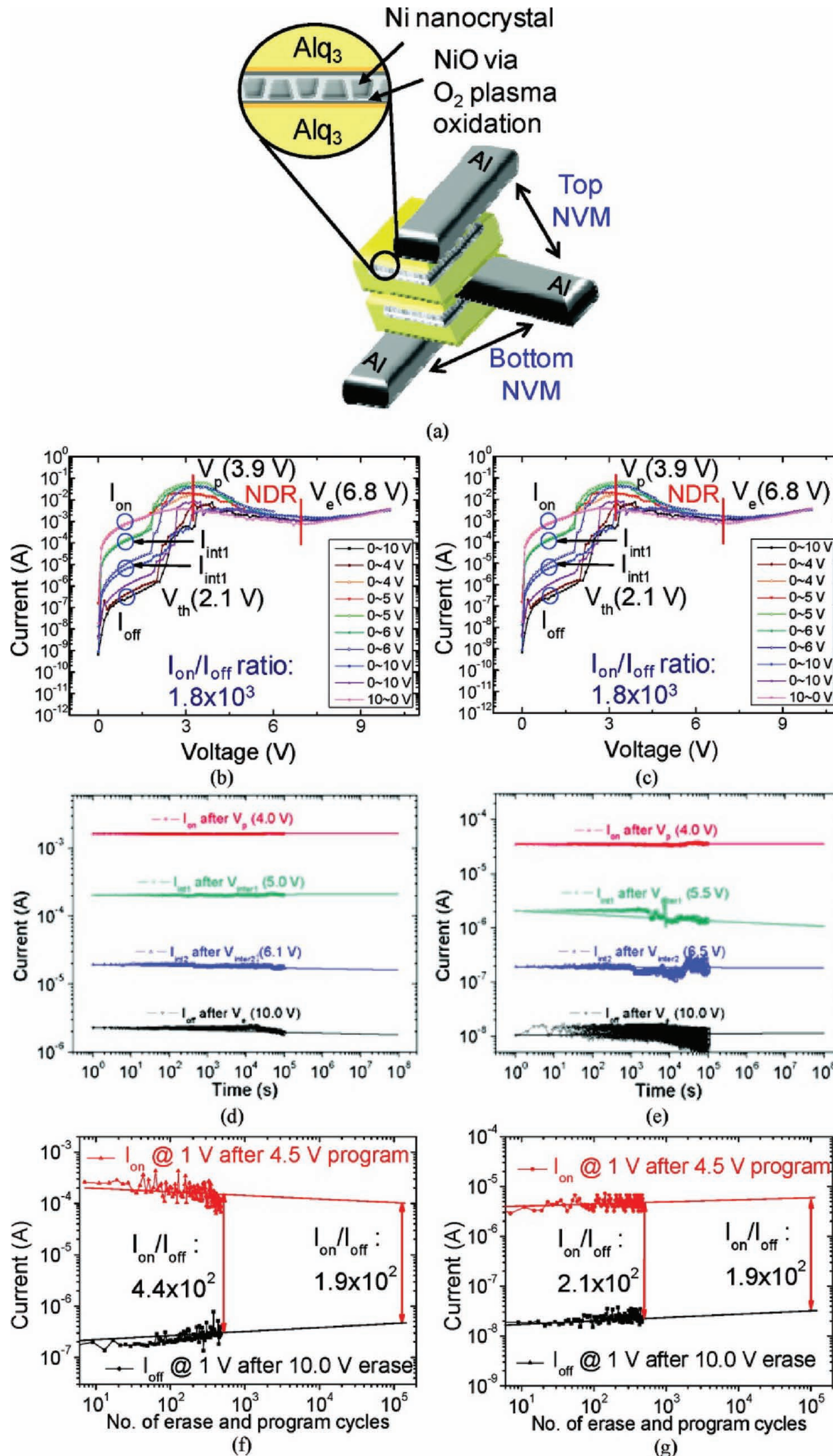

Figure 17. Electrical characteristics of a vertically double-stacked small-molecule nonvolatile $4F^2$ memory cell: a) perspective view of the memory cell. Lower memory cell: b) DC *I–V* curves, d) DC retention, and f) DC endurance. Upper memory cell: c) DC *I–V* curves, e) DC retention, and g) DC endurance. Reproduced with permission.[70] Copyright 2010, American Chemical Society.

© 2011 WILEY-VCH Verlag GmbH & Co. KGaA, Weinheim

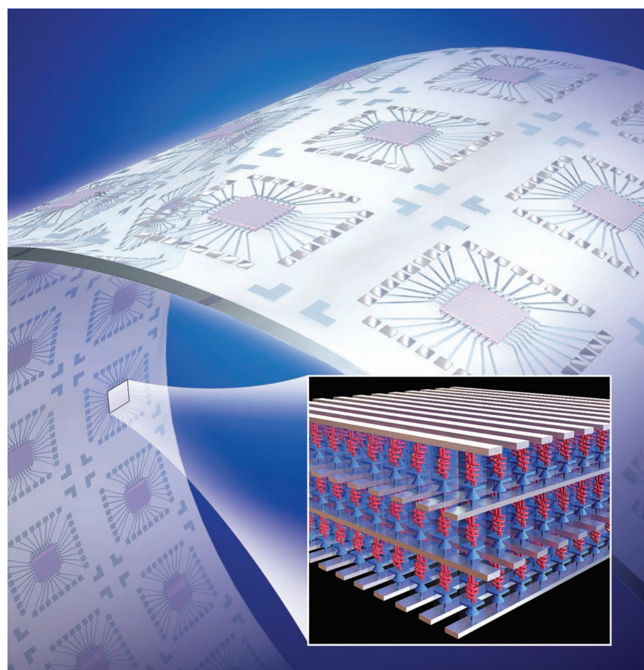

Figure 18. Active matrix system (1D-1R) three-dimensionally stacked on a flexible substrate, representing the most advanced organic resistive memory devices incorporating individual advanced architectural concepts such as 1D-1R, flexibility, and stackability.

cells in each layer was examined (Figure 16b). The ON current values were distributed in a range of approximately one order of magnitude, while the OFF current values were more broadly distributed. However, the ON and OFF currents were distinctly separated by more than one order of magnitude. The statistical distributions of the threshold voltages of the operative memory cells in each layer were also investigated (Figure 16c). The threshold voltage ranges of each layer were similar, indicating that all individual cells could be programmed with a uniform parameter. This study provided a simple and straightforward method for increasing cell density without the use of a complicated downscaling process.

Applying both a vertical stacking structure and the multi-bit concept on a single-chip device can maximize cell density. Using this concept, Park et al.[70] developed a vertically double-stacked $4F^2$ memory cell consisting of Al/AlQ_3/Ni nanocrystals surrounded by a NiO tunneling barrier/Alq3/Al structure (**Figure 17**a). Furthermore, the memory device exhibited four conductivity states. The lower and upper memory cells demonstrated excellent multi-bit operation and produced four stable current states. The intermediate states between the ON and OFF states could be obtained by applying a certain voltage in the NDR region to the device (Figures 17b and 17c). The DC retention times obtained from the lower and upper memory cells are shown in Figures 17d and 17e. Four reading current states at 1.0 V were stable for 10^5 s without any serious degradation, and this time could be extended to 10 years. The DC endurances of the lower and upper memory cells were also measured (Figures 17f and 17g). A memory margin of approximately 10^2 was sustained for 500 cycles. After 10^5 cycles, a high ON/OFF ratio of 1.9×10^2 was expected, indicating stable and reliable memory performance. The authors reported that the retention time characteristic was improved due to Ni nanocrystal with a deep work function, and the stable endurance characteristic was ascribed to a chemically reactive interface between the small molecule (Alq3) layer and the NiO tunneling barrier. Thus, these researchers used vertical stacking and the multi-bit concept to successfully demonstrate extremely high cell densities.

4. Conclusions and Perspective

A decade ago, organic resistive memory devices attracted a substantial amount of attention from scientists and engineers working in organic electronics due to their excellent memory performances and low production costs. The resistive switching phenomena of a variety of organic materials have been correspondingly demonstrated, and switching mechanisms have been proposed based on valid experimental evidence and well-established conduction theories. In the opening sections of this review article, we provided a brief summary of the materials, structures, electrical characteristics, and switching mechanisms associated with two-terminal-based organic memory devices. The objectives of this review were to report the current status of research and development on this emerging memory technology and to present guidelines for viable memory technologies. In particular, we highlighted essential strategies to promote memory performance enhancement, high-density integration, and advanced architectures for future memory applications. Active matrix systems (1D-1R) three-dimensionally stacked on flexible substrates, as schematically illustrated in Figure 18, represent most advanced organic resistive memory devices incorporating individual advanced architectural concepts proposed in this article, which would be our final goal in the technology development roadmap of the organic memory devices.

Despite considerable progress in the advancement of novel memory technologies in recent years, there remain some challenging tasks to be resolved. The first mission is to comprehensively understand the causes of resistance transition. Although several mechanisms (Section 2.2) have been partially established, all observed results have not yet been thoroughly explained. The development of realistic devices hinges on an understanding of the fundamental science behind switching phenomena. Another important mission is to develop fabrication techniques that improve device reproducibility and consequently reduce deviations in electrical characteristics. Identifying and systematizing critical fabrication parameters for the control and optimization of switching characteristics is central to this effort. Furthermore, correlations between the memory parameters (ON/OFF ratio, retention time, cycling endurance, switching speed, and so on) should be investigated to optimize memory performance. Organic resistive memory devices are not likely to replace completely conventional flash memory devices. However, by resolving the scientific and technical issues described above, we believe organic memory technologies will facilitate the development of new flexible memory applications.

© 2011 WILEY-VCH Verlag GmbH & Co. KGaA, Weinheim

Acknowledgements

This work was supported by the National Research Laboratory program, a National Core Research Center grant, the World Class University program of the Korean Ministry of Education, Science and Technology, the Program for Integrated Molecular Systems/GIST, and the IT R&D program of MKE/KEIT.

Received: March 29, 2011
Published online: July 8, 2011

[1] N. Setter, D. Damjanovic, L. Eng, G. Fox, S. Gevorgian, S. Hong, A. Kingon, H. Kohlstedt, N. Y. Park, G. B. Stephenson, I. Stolitchnov, A. K. Taganstev, D. V. Taylor, T. Yamada, S. Streiffer, *J. Appl. Phys.* **2006**, *100*, 051606.
[2] J. D. Boeck, W. V. Roy, J. Das, V. Motsnyi, Z. Liu, L. Lagae, H. Boeve, K. Dessein, G. Borghs, *Semicond. Sci. Technol.* **2002**, *17*, 342.
[3] S. Hudgens, B. Johnson, *MRS Bull.* **2004**, *29*, 829.
[4] R. Waser, M. Aono, *Nat. Mater.* **2007**, *6*, 833.
[5] S. Tehrani, J. M. Slaughter, E. Chen, M. Durlam, J. Shi, M. DeHerren, *IEEE Trans. Magn.* **1999**, *35*, 2814.
[6] H. Y. Jeong, Y. I. Kim, J. Y. Lee, S.-Y. Choi, *Nanotechnology* **2010**, *21*, 115203.
[7] L. P. Ma, J. Liu, Y. Yang, *Appl. Phys. Lett.* **2002**, *80*, 2997.
[8] J. Ouyang, C.-W. Chu, C. R. Szmanda, L. Ma, Y. Yang, *Nat. Mater.* **2004**, *3*, 918.
[9] C. W. Chu, J. Ouyang, J. H. Tseng, Y. Yang, *Adv. Mater.* **2005**, *17*, 1440.
[10] R. J. Tseng, J. Huang, J. Ouyang, R. B. Kaner, Y. Yang, *Nano Lett.* **2005**, *5*, 1077.
[11] R. J. Tseng, C. Tsai, L. Ma, J. Ouyang, C. S. Ozkan, Y. Yang, *Nat. Nanotechnol.* **2006**, *1*, 72.
[12] Y. Yang, J. Ouyang, L. Ma, R. J. H. Tseng, C. W. Chu, *Adv. Funct. Mat.* **2006**, *16*, 1001.
[13] J. C. Scott, L. D. Bozano, *Adv. Mater.* **2007**, *19*, 1452.
[14] Q.-D. Ling, D.-J. Liaw, C. Zhu, D. S.-H. Chan, E.-T. Kang, K.-G. Neoh, *Prog. Polym. Sci.* **2008**, *33*, 917.
[15] B. Mukherjee, A. J. Pal, *Org. Electron.* **2006**, *7*, 249.
[16] T. Kondo, S. M. Lee, M. Malicki, B. Domercq, S. R. Marder, B. Kippelen, *Adv. Funct. Mat.* **2008**, *18*, 1112.
[17] X.-D. Zhuang, Y. Chen, G. Liu, B. Zhang, K.-G. Neoh, E.-T. Kang, C.-X. Zhu, Y.-X. Li, L.-J. Niu, *Adv. Funct. Mat.* **2010**, *20*, 2916.
[18] B. Cho, S. Song, Y. Ji, T. Lee, *Appl. Phys. Lett.* **2010**, *97*, 063305.
[19] P. Y. Lai, J. S. Chen, *Appl. Phys. Lett.* **2008**, *93*, 153305.
[20] Y. Li, D. Qiu, L. Cao, C. Shao, L. Pan, L. Pu, J. Xu, Y. Shi, *Appl. Phys. Lett.* **2010**, *96*, 133303.
[21] B.-O. Cho, T. Yasue, H. Yoon, M.-S. Lee, I.-S. Yeo, U. I. Chung, J.-T. Moon, B.-I. Ryu, *IEEE Int. Electron Devices Meet.* **2006**, 21, DOI: 10.1109/IEDM.2006.346729.
[22] J. Chen, D. Ma, *J. Appl. Phys.* **2006**, *100*, 034512.
[23] J. Lin, D. Ma, *J. Appl. Phys.* **2008**, *103*, 024507.
[24] G. Liu, Q.-D. Ling, E.-T. Kang, K.-G. Neoh, D.-J. Liaw, F.-C. Chang, C.-X. Zhu, D. S.-H. Chan, *J. Appl. Phys.* **2007**, *102*, 024502.
[25] J. Bo, W. Zhaoxin, H. Qiang, T. Yuan, M. Guilin, H. Xun, *J. Phys. D: Appl. Phys.* **2010**, *43*, 035101.
[26] T.-W. Kim, S.-H. Oh, J. Lee, H. Choi, G. Wang, J. Park, D.-Y. Kim, H. Hwang, T. Lee, *Org. Electron.* **2010**, *11*, 109.
[27] B. Lei, W. L. Kwan, Y. Shao, Y. Yang, *Org. Electron.* **2009**, *10*, 1048.
[28] J. Lin, D. Ma, *Org. Electron.* **2009**, *10*, 275.
[29] G. Liu, Q.-D. Ling, E. Y. H. Teo, C.-X. Zhu, D. S.-H. Chan, K.-G. Neoh, E.-T. Kang, *ACS Nano* **2009**, *3*, 1929.
[30] L. D. Bozano, B. W. Kean, M. Beinhoff, K. R. Carter, P. M. Rice, J. C. Scott, *Adv. Funct. Mat.* **2005**, *15*, 1933.
[31] T.-W. Kim, S.-H. Oh, H. Choi, G. Wang, H. Hwang, D.-Y. Kim, T. Lee, *Appl. Phys. Lett.* **2008**, *92*, 253308.
[32] H.-T. Lin, Z. Pei, Y.-J. Chan, *IEEE Electron Device Lett.* **2007**, *28*, 569.
[33] J.-R. Chen, H.-T. Lin, G.-W. Hwang, Y.-J. Chan, P.-W. Li, *Nanotechnology* **2009**, *20*, 255706.
[34] K. Asadi, D. M. de Leeuw, B. de Boer, P. W. M. Blom, *Nat. Mater.* **2008**, *7*, 547.
[35] Z. J. Donhauser, B. A. Mantooth, K. F. Kelly, L. A. Bumm, J. D. Monnell, J. J. Stapleton, D. W. Price, A. M. Rawlett, D. L. Allara, J. M. Tour, P. S. Weiss, *Science* **2001**, *292*, 2303.
[36] G. Peng, D. Yuan-Wei, J. Xin, L. Yin-Xiang, X. Wei, *IEEE Electron Device Lett.* **2007**, *28*, 572.
[37] C. N. Lau, D. R. Stewart, R. S. Williams, M. Bockrath, *Nano Lett.* **2004**, *4*, 569.
[38] B. C. Das, A. J. Pal, *Org. Electron.* **2008**, *9*, 39.
[39] H. Carchano, R. Lacoste, Y. Segui, *Appl. Phys. Lett.* **1971**, *19*, 414.
[40] H. K. Henisch, W. R. Smith, *Appl. Phys. Lett.* **1974**, *24*, 589.
[41] S. L. Lim, Ling, E. Y. H. Teo, C. X. Zhu, D. S. H. Chan, Kang, K. G. Neoh, *Chem. Mater.* **2007**, *19*, 5148.
[42] T.-W. Kim, S.-H. Oh, H. Choi, G. Wang, H. Hwang, D.-Y. Kim, T. Lee, *IEEE Electron Device Lett.* **2008**, *29*, 852.
[43] H. S. Majumdar, A. Bandyopadhyay, A. Bolognesi, A. J. Pal, *J. Appl. Phys.* **2002**, *91*, 2433.
[44] Y. Sadaoka, Y. Sakai, *J. Chem. Soc., Faraday Trans. 2* **1976**, *72*, 1911.
[45] S. H. Kim, K. S. Yook, J. Jang, J. Y. Lee, *Synth. Methods* **2008**, *158*, 861.
[46] A. Laiho, H. S. Majumdar, J. K. Baral, F. Jansson, R. Osterbacka, O. Ikkala, *Appl. Phys. Lett.* **2008**, *93*, 203309.
[47] F. Li, T. W. Kim, W. Dong, Y.-H. Kim, *Appl. Phys. Lett.* **2008**, *92*, 011906.
[48] F. Li, D.-I. Son, S.-M. Seo, H.-M. Cha, H.-J. Kim, B.-J. Kim, J. H. Jung, T. W. Kim, *Appl. Phys. Lett.* **2007**, *91*, 122111.
[49] D. T. Simon, M. S. Griffo, R. A. DiPietro, S. A. Swanson, S. A. Carter, *Appl. Phys. Lett.* **2006**, *89*, 133510.
[50] F. Verbakel, S. C. J. Meskers, R. A. J. Janssen, *Chem. Mater.* **2006**, *18*, 2707.
[51] Y. Song, Q. D. Ling, S. L. Lim, E. Y. H. Teo, Y. P. Tan, L. Li, E. T. Kang, D. S. H. Chan, C. Zhu, *IEEE Electron Device Lett.* **2007**, *28*, 107.
[52] S. Paul, A. Kanwal, M. Chhowalla, *Nanotechnology* **2006**, *17*, 145.
[53] D.-I. Son, J.-H. Kim, D.-H. Park, W. K. Choi, F. Li, J. H. Ham, T. W. Kim, *Nanotechnology* **2008**, *19*, 055204.
[54] A. Bandyopadhyay, A. J. Pal, *Appl. Phys. Lett.* **2004**, *84*, 999.
[55] M. Nakaya, S. Tsukamoto, Y. Kuwahara, M. Aono, T. Nakayama, *Adv. Mater.* **2010**, *22*, 1622.
[56] J. Lee, H. Chang, S. Kim, G. S. Bang, H. Lee, *Angew. Chem. Int. Ed.* **2009**, *48*, 8501.
[57] A. Bandyopadhyay, A. J. Pal, *Appl. Phys. Lett.* **2003**, *82*, 1215.
[58] S. Y. Quek, M. Kamenetska, M. L. Steigerwald, H. J. Choi, S. G. Louie, M. S. Hybertsen, J. B. Neaton, VenkataramanLatha, *Nat. Nanotechnol.* **2009**, *4*, 230.
[59] B. Cho, T.-W. Kim, M. Choe, G. Wang, S. Song, T. Lee, *Org. Electron.* **2009**, *10*, 473.
[60] T. J. Lee, S. Park, S. G. Hahm, D. M. Kim, K. Kim, J. Kim, W. Kwon, Y. Kim, T. Chang, M. Ree, *J. Phys. Chem. C* **2009**, *113*, 3855.
[61] E. Y. H. Teo, Q. D. Ling, Y. Song, Y. P. Tan, W. Wang, E. T. Kang, D. S. H. Chan, C. Zhu, *Org. Electron.* **2006**, *7*, 173.
[62] S. Möller, C. Perlov, W. Jackson, C. Taussig, S. R. Forrest, *Nature* **2003**, *426*, 166.
[63] V. S. Reddy, S. Karak, A. Dhar, *Appl. Phys. Lett.* **2009**, *94*, 173304.
[64] J. Ouyang, Y. Yang, *Appl. Phys. Lett.* **2010**, *96*, 063506.
[65] B. Cho, T.-W. Kim, S. Song, Y. Ji, M. Jo, H. Hwang, G.-Y. Jung, T. Lee, *Adv. Mater.* **2010**, *22*, 1228.

 © 2011 WILEY-VCH Verlag GmbH & Co. KGaA, Weinheim

[66] M. J. Lee, Y. Park, D. S. Suh, E. H. Lee, S. Seo, D. C. Kim, R. Jung, B. S. Kang, S. E. Ahn, C. B. Lee, D. H. Seo, Y. K. Cha, I. K. Yoo, J. S. Kim, B. H. Park, *Adv. Mater.* **2007**, *19*, 3919.
[67] H.-T. Lin, Z. Pei, J.-R. Chen, Y.-J. Chan, *IEEE Electron Device Lett.* **2009**, *30*, 18.
[68] I. G. Baek, D. C. Kim, M. J. Lee, H. J. Kim, E. K. Yim, M. S. Lee, J. E. Lee, S. E. Ahn, S. Seo, J. H. Lee, J. C. Park, Y. K. Cha, S. O. Park, H. S. Kim, I. K. Yoo, U. I. Chung, J. T. Moon, B. I. Ryu, *IEEE Int. Electron Devices Meet.* **2005**, 750, DOI: 10.1109/IEDM.2005.1609462
[69] L. Li, Q.-D. Ling, S.-L. Lim, Y.-P. Tan, C. Zhu, D. S. H. Chan, E.-T. Kang, K.-G. Neoh, *Org. Electron.* **2007**, *8*, 401.
[70] J.-G. Park, W.-S. Nam, S.-H. Seo, Y.-G. Kim, Y.-H. Oh, G.-S. Lee, U.-G. Paik, *Nano Lett.* **2009**, *9*, 1713.
[71] D. Attianese, M. Petrosino, P. Vacca, S. Concilio, P. Iannelli, A. Rubino, S. Bellone, *IEEE Electron Device Lett.* **2008**, *29*, 44.
[72] E. H. Rhoderick, R. H. Williams, *Metal-Semiconductor Contacts*, 2nd ed. Oxford University Press, Oxford, **1988**
[73] W. Tang, H. Shi, G. Xu, B. S. Ong, Z. D. Popovic, J. Deng, J. Zhao, G. Rao, *Adv. Mater.* **2005**, *17*, 2307.
[74] J. H. A. Smits, S. C. J. Meskers, R. A. J. Janssen, A. W. Marsman, D. M. de Leeuw, *Adv. Mater.* **2005**, *17*, 1169.
[75] W.-J. Joo, T.-L. Choi, K.-H. Lee, Y. Chung, *J. Phys. Chem. B* **2007**, *111*, 7756.
[76] G. Dearnaley, A. M. Stoneham, D. V. Morgan, *Rep. Prog. Phys.* **1970**, *33*, 1129.
[77] L. F. Pender, R. J. Fleming, *J. Appl. Phys.* **1975**, *46*, 3426.
[78] Y. Segui, B. Ai, H. Carchano, *J. Appl. Phys.* **1976**, *47*, 140.
[79] G. Dearnaley, D. V. Morgan, A. M. Stoneham, *J. Non-Cryst. Solids* **1970**, *4*, 593.
[80] W. Hwang, K. C. Kao, *J. Chem. Phys.* **1974**, *60*, 3845.
[81] S. Sivaramakrishnan, P.-J. Chia, Y.-C. Yeo, L.-L. Chua, P. K. H. Ho, *Nat. Mater.* **2007**, *6*, 149.
[82] W.-J. Joo, T.-L. Choi, J. Lee, S. K. Lee, M.-S. Jung, N. Kim, J. M. Kim, *J. Phys. Chem. B* **2006**, *110*, 23812.
[83] T.-W. Kim, H. Choi, S.-H. Oh, M. Jo, G. Wang, B. Cho, D.-Y. Kim, H. Hwang, T. Lee, *Nanotechnology* **2009**, *20*, 025201.
[84] A. Carbone, B. K. Kotowska, D. Kotowski, *Phys. Rev. Lett.* **2005**, *95*, 236601.
[85] P. Mark, W. Helfrich, *J. Appl. Phys.* **1962**, *33*, 205.
[86] S. Das, A. J. Pal, *Appl. Phys. Lett.* **2000**, *76*, 1770.
[87] L. D. Bozano, B. W. Kean, V. R. Deline, J. R. Salem, J. C. Scott, *Appl. Phys. Lett.* **2004**, *84*, 607.
[88] J. G. Simmons, R. R. Verderber, *Proc. R. Soc. London, Ser. A* **1967**, *301*, 77.
[89] R. S. Potember, T. O. Poehler, D. O. Cowan, *Appl. Phys. Lett.* **1979**, *34*, 405.
[90] E. I. Kamitsos, C. H. Tzinis, W. M. Risen, *Solid State Commun.* **1982**, *42*, 561.
[91] B. Mukherjee, A. J. Pal, *Synth. Methods* **2005**, *155*, 336.
[92] H. Ma, H.-L. Yip, F. Huang, A. K. Y. Jen, *Adv. Funct. Mat.* **2010**, *20*, 1371.
[93] A. Bandyopadhyay, A. J. Pal, *Adv. Mater.* **2003**, *15*, 1949.
[94] M. Cölle, M. Büchel, D. M. de Leeuw, *Org. Electron.* **2006**, *7*, 305.
[95] K. S. Yook, J. Y. Lee, S. H. Kim, J. Jang, *Appl. Phys. Lett.* **2008**, *92*, 223305.
[96] F. Verbakel, S. C. J. Meskers, R. A. J. Janssen, H. L. Gomes, M. Cölle, M. Büchel, D. M. de Leeuw, *Appl. Phys. Lett.* **2007**, *91*, 192103.
[97] A. C. Durr, F. Schreiber, M. Kelsch, H. D. Carstanjen, H. Dosch, O. H. Seeck, *J. Appl. Phys.* **2003**, *93*, 5201.
[98] R. Ruiz, D. Choudhary, B. Nickel, T. Toccoli, K.-C. Chang, A. C. Mayer, P. Clancy, J. M. Blakely, R. L. Headrick, S. Iannotta, G. G. Malliaras, *Chem. Mater.* **2004**, *16*, 4497.
[99] J. Chen, D. Ma, *Appl. Phys. Lett.* **2005**, *87*, 023505.
[100] S. Pyo, L. Ma, J. He, Q. Xu, Y. Yang, Y. Gao, *J. Appl. Phys.* **2005**, *98*, 054303.
[101] M. Uchida, C. Adachi, T. Koyama, Y. Taniguchi, *J. Appl. Phys.* **1999**, *86*, 1680.
[102] S.-H. Oh, S.-I. Na, Y.-C. Nah, D. Vak, S.-S. Kim, D.-Y. Kim, *Org. Electron.* **2007**, *8*, 773.
[103] G. Pfister, C. H. Griffiths, *Phys. Rev. Lett.* **1978**, *40*, 659.
[104] P. G. Lecomber, A. E. Owen, W. E. Spear, J. Hajto, A. J. Snell, W. K. Choi, M. J. Rose, S. Reynolds, *J. Non-Cryst. Solids* **1985**, *77–78*1373.
[105] M. Geissler, H. Wolf, R. Stutz, E. Delamarche, U.-W. Grummt, B. Michel, A. Bietsch, *Langmuir* **2003**, *19*, 6301.
[106] Y.-L. Loo, R. L. Willett, K. W. Baldwin, J. A. Rogers, *J. Am. Chem. Soc.* **2002**, *124*, 7654.
[107] T.-W. Kim, K. Lee, S.-H. Oh, G. Wang, D.-Y. Kim, G.-Y. Jung, T. Lee, *Nanotechnology* **2008**, *19*, 405201.
[108] G.-Y. Jung, Z. Li, W. Wu, Y. Chen, D. L. Olynick, S.-Y. Wang, W. M. Tong, R. S. Williams, *Langmuir* **2005**, *21*, 1158.
[109] K. Lee, S.-H. Oh, N.-G. Kang, J.-S. Lee, D.-Y. Kim, H. Lee, G. Y. Jung, *Langmuir* **2008**, *24*, 8413.
[110] M. Lauters, B. McCarthy, D. Sarid, G. E. Jabbour, *Appl. Phys. Lett.* **2006**, *89*, 013507.
[111] C. Jiangshan, X. Liling, L. Jian, G. Yanhou, W. Lixiang, M. Dongge, *Semicond. Sci. Technol.* **2006**, *21*, 1121.
[112] G. Yang, H.-Y. Chen, L. Ma, Y. Shao, Y. Yang, *Appl. Phys. Lett.* **2009**, *95*, 203506.
[113] N. F. Mott, *Adv. Phys.* **1967**, *16*, 49.
[114] E. G. Gerstner, D. R. McKenzie, *J. Appl. Phys.* **1998**, *84*, 5647.
[115] C. Laurent, E. Kay, N. Souag, *J. Appl. Phys.* **1988**, *64*, 336.
[116] K. Kinoshita, K. Tsunoda, Y. Sato, H. Noshiro, S. Yagaki, M. Aoki, Y. Sugiyama, *Appl. Phys. Lett.* **2008**, *93*, 033506.
[117] J. C. Scott, *Science* **2004**, *304*, 62.
[118] International Technology Roadmap for Semiconductors **2007**, http://www.itrs.net/Links/2007ITRS/Home2007.htm
[119] E. Y. H. Teo, C. Zhang, S. L. Lim, E.-T. Kang, D. S. H. Chan, C. Zhu, *IEEE Electron Device Lett.* **2009**, *30*, 487.
[120] S.-E. Ahn, B. S. Kang, K. H. Kim, M.-J. Lee, C. B. Lee, G. Stefanovich, C. J. Kim, Y. Park, *IEEE Electron Device Lett.* **2009**, *30*, 550.
[121] T.-W. Kim, H. Choi, S.-H. Oh, G. Wang, D.-Y. Kim, H. Hwang, T. Lee, *Adv. Mater.* **2009**, *21*, 2497.
[122] B. S. Kang, S.-E. Ahn, M.-J. Lee, G. Stefanovich, K. H. Kim, W. X. Xianyu, C. B. Lee, Y. Park, I. G. Baek, B. H. Park, *Adv. Mater.* **2008**, *20*, 3066.
[123] M.-J. Lee, S. I. Kim, C. B. Lee, H. Yin, S.-E. Ahn, B. S. Kang, K. H. Kim, J. C. Park, C. J. Kim, I. Song, S. W. Kim, G. Stefanovich, J. H. Lee, S. J. Chung, Y. H. Kim, Y. Park, *Adv. Funct. Mat.* **2009**, *19*, 1587.
[124] K. Asadi, M. Li, N. Stingelin, P. W. M. Blom, D. M. de Leeuw, *Appl. Phys. Lett.* **2010**, *97*, 193308.
[125] S. Kim, Y.-K. Choi, *Appl. Phys. Lett.* **2008**, *92*, 223508.
[126] S. Lee, H. Kim, D.-J. Yun, S.-W. Rhee, K. Yong, *Appl. Phys. Lett.* **2009**, *95*, 262113.
[127] H. Y. Jeong, J. Y. Kim, J. W. Kim, J. O. Hwang, J.-E. Kim, J. Y. Lee, T. H. Yoon, B. J. Cho, S. O. Kim, R. S. Ruoff, S.-Y. Choi, *Nano Lett.* **2010**, *10*, 4381.
[128] Y. Ji, B. Cho, S. Song, T.-W. Kim, M. Choe, Y. H. Kahng, T. Lee, *Adv. Mater.* **2010**, *22*, 3071.
[129] A. SarI, K. Kaygusuz, *Renewable Energy* **2003**, *28*, 939.
[130] Y. C. Yang, F. Pan, Q. Liu, M. Liu, F. Zeng, *Nano Lett.* **2009**, *9*, 1636.
[131] M.-J. Lee, S. Han, S. H. Jeon, B. H. Park, B. S. Kang, S.-E. Ahn, K. H. Kim, C. B. Lee, C. J. Kim, I.-K. Yoo, D. H. Seo, X.-S. Li, J.-B. Park, J.-H. Lee, Y. Park, *Nano Lett.* **2009**, *9*, 1476.

© 2011 WILEY-VCH Verlag GmbH & Co. KGaA, Weinheim

[132] T. Sekitani, T. Yokota, U. Zschieschang, H. Klauk, S. Bauer, K. Takeuchi, M. Takamiya, T. Sakurai, T. Someya, *Science* **2009**, *326*, 1516.
[133] K. Lian, R. Li, H. Wang, J. Zhang, D. Gamota, *Mater. Sci. Eng. B* **2010**, *167*, 12.
[134] A. J. Heeger, *Angew. Chem. Int. Ed.* **2001**, *40*, 2591.
[135] A. G. MacDiarmid, *Angew. Chem. Int. Ed.* **2001**, *40*, 2581.
[136] S. Song, B. Cho, T.-W. Kim, Y. Ji, M. Jo, G. Wang, M. Choe, Y. H. Kahng, H. Hwang, T. Lee, *Adv. Mater.* **2010**, *22*, 5048.
[137] W. L. Kwan, R. J. Tseng, W. Wu, Q. Pei, Y. Yang, *IEEE Int. Electron Devices Meet.* **2007**, 237, DOI: 10.1109/IEDM.2007.4418911.
[138] W. L. Kwan, R. J. Tseng, Y. Yang, *Philos. Trans. R. Soc., A* **2009**, *367*, 4159.
[139] C. Kügeler, M. Meier, R. Rosezin, S. Gilles, R. Waser, *Solid-State Electron.* **2009**, *53*, 1287.

© 2011 WILEY-VCH Verlag GmbH & Co. KGaA, Weinheim

CORRECTIONS

Organic Resistive Memory Devices: Performance Enhancement, Integration, and Advanced Architectures

*Byungjin Cho, Sunghun Song, Yongsung Ji, Tae-Wook Kim, and Takhee Lee**

Adv. Funct. Mater. **2011**, *21*, 2806–2829.

DOI: 10.1002/adfm.201100686

The authors regret a mistake in the list of contributing authors. The first name of Sunghun Song is misspelled; the correct name is Sunghoon Song.

The corrected byline should read:

*Byungjin Cho, Sunghoon Song, Yongsung Ji, Tae-Wook Kim, and Takhee Lee**

 © 2011 WILEY-VCH Verlag GmbH & Co. KGaA, Weinheim